Effective ionisation coefficients and critical breakdown electric field of CO_2 at elevated temperature : effect of excited states and ion kinetics

Reference:

Wang Weizong, Bogaerts Annemie.- Effective ionisation coefficients and critical breakdown electric field of CO_2 at elevated temperature : effect of excited states and ion kinetics

Plasma sources science and technology / Institute of Physics - ISSN 0963-0252 - 25:5(2016), p. 1-22

Full text (Publishers DOI): http://dx.doi.org/doi:10.1088/0963-0252/25/5/055025

Effective ionisation coefficients and critical breakdown electric field of CO_2 at elevated temperature: Effect of excited states and ion kinetics

Weizong Wang* and Annemie Bogaerts

Research group PLASMANT, Department of Chemistry, University of Antwerp, Universiteitsplein 1, B-2610 Wilrijk-Antwerp, Belgium

E-mail: wangweizong@gmail.com, annemie.bogaerts@uantwerpen.be

Abstract:

Electrical breakdown by the application of an electric field occurs more easily in hot gases than in cold gases because of the extra electron-species interactions that occur as a result of dissociation, ionization and excitation at higher temperature. This paper discusses some overlooked physics and clarifies inaccuracies in the evaluation of the effective ionization coefficients and the critical reduced breakdown electric field of CO_2 at elevated temperature, considering the influence of excited states and ion kinetics. The critical reduced breakdown electric field is obtained by balancing electron generation and loss mechanisms using the electron energy distribution function (EEDF) derived from the Boltzmann transport equation under the two-term approximation. The equilibrium compositions of the hot gas mixtures are determined based on Gibbs free energy minimization considering the ground states as well as vibrationally and electronically excited states as independent species, which follow a Boltzmann distribution with a fixed excitation temperature. The interaction cross sections between electrons and the excited species, not reported previously, are properly taken into account. Furthermore, the ion kinetics, including electron-ion recombination, associative electron detachment, charge transfer and ion conversion into stable negative ion clusters, are also considered. Our results indicate that the excited species lead to a greater population of high-energy electrons at higher gas temperature and this affects the Townsend rate coefficients (i.e., of electron impact ionization and attachment), but the critical reduced breakdown electric field strength of CO_2 is only affected when also properly accounting for the ion kinetics. Indeed, the latter greatly influences the effective ionization coefficients and hence the critical reduced breakdown electric field at temperatures above 1500K. The rapid increase of the dissociative electron attachment cross-section of molecular oxygen upon rising vibrational quantum number leads to a larger electron loss rate and this enhances the critical reduced breakdown electric field strength in the temperature range where the concentration of molecular oxygen is relatively high. The results obtained in this work show reasonable agreement with experimental results from literature, and are important for the evaluation of the dielectric strength of CO_2 in a highly reactive environment at elevated temperature.

Keywords: CO_2, excited species, ion kinetics, effective ionization coefficients, critical breakdown electric field, electron energy distribution function, Boltzmann equation

Submitted to Plasma Sources Science and Technology

1. Introduction

Understanding the dielectric properties of a hot gas is required for various practical applications because electric breakdown often takes place at elevated temperature. For example, in a circuit breaker, if the hot gas between both electrodes that is left behind by the thermally-recovered arc has a lower dielectric strength than the applied electric field strength, an electrical breakdown of the hot gas occurs, causing reignition of the arc and interruption failure[1]-[3]. Another example where this is important is a gliding arc, which is an auto-oscillating periodic discharge between two diverging electrodes, and which is considered as one of the most effective and promising plasmas for the conversion of greenhouse gases into value-added chemicals. The arc grows with rising interelectrode distance until it extinguishes. At that moment the discharge reignites itself at the shortest electrode gap separation, where a residual warm environment facilitates the start of a new cycle [4]-[5]. The gas breakdown depends on whether an electron avalanche can be formed for a given electric field. The formation of an electron avalanche is determined by the production and loss processes of electrons. Electron impact ionization and electron detachment contribute to the production of electrons, while electron attachment and recombination with ions are responsible for their loss. A Townsend avalanche usually develops from the initiating electron. The total number of electrons in the avalanche initiated at x = 0 from N_0 initial electrons (often $N_0 = 1$) is described by

$$N_e(x) = N_0 \exp(K(x)) \tag{1}$$

where the ionization integral K(x) is defined as

$$K(x) = \int_0^x \alpha_{eff}(x')dx' \tag{2}$$

Here α_{eff} is known as the effective Townsend ionization coefficient, expressed in m^{-1}, and defined as the number of electrons produced by one electron per unit length in the direction of the electric field.

Critical reduced breakdown electric field strengths, at which the production and loss of charged species is exactly balanced and the effective ionization coefficient is zero, have been widely studied by both numerical calculations and experiments for various gases at room temperature [6]-[17]. However, detailed experimental investigations for hot gases have rarely been performed because these phenomena are complicated and therefore difficult to treat at elevated temperature. Eliasson and Schade [18]-[19] have reported experimental results for the breakdown voltage of hot SF_6. Rothhardt et al. have experimentally measured the temperature dependence of the breakdown voltage of air, N_2 and SF_6 up to 3500 K [20]-[22]. Uchii et al. performed breakdown voltage measurements inside a circuit breaker which led to an estimate of the gas temperature [23].

Besides experiments, theoretical studies by means of the Boltzmann equation should be able to provide valuable information on the dielectric properties of hot gases and gas mixtures, and they have recently become a research hotspot [24]-[33]. In fact, if the ion kinetics is not taken into account, i.e., electron-ion recombination

and electron detachment from negative ions are neglected, the effective ionization coefficient is simply determined from the Townsend ionization coefficient α and the Townsend electron attachment coefficient η as

$$\alpha_{eff} = \alpha - \eta \tag{3}$$

The Townsend coefficients α and η are also expressed in m^{-1}, and they represent the number of electrons formed or lost per unit length and normalized per electron, due to electron impact ionization and electron attachment, respectively. They can be determined from the ionization and attachment rate coefficients, which are calculated from the electron energy distribution function (EEDF) based on the collision cross section sets and the number densities of all species present in the dissociated gas. Note that the role of ions becomes significant at higher temperature, the electron kinetics alone by formula (3) is not sufficient to obtain reliable data on the effective ionization coefficients and on the critical reduced breakdown electric field strength. Therefore, the ions kinetics, which play an important role above 1500 K, and which have also not yet been considered in the existing literature should be taken into account in the evaluation of hot gas breakdown.

To our knowledge, all previous calculations of critical reduced breakdown electric field strength have neglected the role of vibrationally and electronically excited species and this will definitely bring some deviation in the estimated critical reduced breakdown electric field strength. Indeed, the excited species may have different interaction behavior with electrons, and their population might even be higher than the ground state species, for a certain temperature and gas pressure (see below). Colonna et al. [34] calculated the reduced electric fields responsible for electrical breakdown in high temperature air by solving a stationary Boltzmann equation including superelastic vibrational collisions, which play an important role in the determination of the electron energy distribution function (EEDF). The authors suggest that the calculation can be further improved by taking into account the dissociative attachment and ionization from vibrationally excited states, because their cross sections have a strong dependence on the vibrational quantum number. Recently, Pietanza et al.[35]-[36] performed a Boltzmann equation analysis for pure CO_2 plasma, in the presence of superelastic vibrational and electronic collisions, as well as electron-electron Coulomb collisions, in both discharge and post-discharge conditions. They also found that the influence of superelastic vibrational collisions on the EEDF in CO_2 is non-negligible.

Therefore, the present aims to evaluate the effective ionization coefficient and critical reduced breakdown electric field strength of CO_2 and its dissociation products at elevated temperatures from 300 K up to 5000 K, and tries to clarify the influence of ion kinetics and excited states on the calculation. This paper is organized as follows: Section 2 presents the species composition of hot CO_2 gas, which is s a prerequisite to obtain the dielectric properties of dissociated CO_2 gas when applying an electric field. Section 3 describes the electron collision processes for both the ground states as well as the vibrationally and electronically excited states considered in this work. The ion kinetics, which plays a significant role in the electron avalanche development at elevated temperature, is described as well. Section 4 gives a theoretical determination of the

effective ionization coefficients and the critical reduced breakdown electric field strength by taking into account both the electron and ions kinetics. The results obtained concerning the physical mechanisms responsible for the breakdown are discussed and compared with available experimental data in Sections 5. Finally appropriate conclusions are drawn.

2. Species composition of hot CO_2 gas

The dissociation of CO_2 takes place at elevated temperature, and the neutral species composition of the gaseous mixture can influence the EEDFs and hence the electron kinetics, as well as the occurrence of breakdown, due to the different collision cross sections (see section 3.1 below). Furthermore, at high temperature, thermal ionization can also occur, producing ions and electrons, which can also influence the ion kinetics and the electron avalanche development (see section 3.2 below). Therefore, determining the species composition is a prerequisite to obtain the dielectric properties of dissociated CO_2 gas when applying an electric field. The various neutral species, positive and negative ions originating from CO_2 at elevated temperature, included in our model, are listed in table 1. Besides the ground states, we also include several vibrational levels and electronically excited levels for the most important neutral species, as shown in table 1. The energies of the vibrational levels of the molecular species are calculated using the anharmonic oscillator approximation [37]. To have an efficient and not excessively complex model, we include only a limited number of vibrational levels, i.e., 8 CO_2, 10 CO and 4 O_2 vibrational levels, and only a few electronically excited states of CO_2, C, O, CO and O_2, as indicated in table 1, primarily to account for the electron energy losses upon excitation to these levels. These excited states are chosen because they have the lowest energy. Electron impact excitation of the ground state to these levels is very important and plays a non-negligible role in reproducing experimental swarm data.

For CO_2, the different vibrational levels are grouped in 8 effective levels, i.e. the first bending mode (010), denoted as CO_2v1, the first asymmetric stretching mode level (001), denoted as CO_2v8, and 6 mixing levels (Fermi resonance levels), represented by v2~v7 (0n0 + n00). The Fermi resonance levels connect symmetric stretching and bending mode levels, which have similar energies, and their states are indicated in a generic way by (0n0) + (n00). The details are listed in table 2 below. Moreover, we also include two electronic excitations with threshold energies at 7.0 and 10.5 eV, respectively. However, the 7 eV threshold energy process is considered as a dissociative channel, and for this reason, only one CO_2 electronically excited level is listed in table 1 and table 2.

For CO, the first 10 vibrational levels (for which the electron impact excitation cross sections are available in the literature) up to an energy of 2.51 eV are included in the model, as well as 5 electronic excitations (See details in table 2 below). For O_2, the 4 vibrational states with the lowest energy levels are taken into account, as well as 5 electronic excitation states, as indicated in table 2 below. For atomic carbon and oxygen, we include two electronic excitation states, i.e., C(1D), C(1S) and O(1D), O(1S), with energies at 1.26 eV, 2.68 eV, 1.97 eV and 4.20 eV, respectively.

Table 1 Overview of the species included in the model. Details on the vibrational and electronic states are given in table 2.

Neutral species	CO_2, CO, C, C_2, O_2, O_3, O
Positive ions	CO_2^+, CO^+, C_2^+, O_2^+, O^+, C^+
Negative ions	CO_3^-, O^-, O_2^-, O_3^-,
Vibrational states	CO_2(8), CO(10), O_2(4)
Electronic states	O(2) , C(2), CO_2(1), CO(5), O_2(5)
Electrons	e^-

Under the ideal condition of local thermal equilibrium, the chemical equilibrium concentration of each species (including ground state and the various vibrational and electronically excited levels) is calculated as a function of temperature and pressure by minimizing the Gibbs energy of the system, which is a standard technique in equilibrium chemistry [38]-[39]. Note that the equilibrium composition obtained by using statistical thermodynamics through partition functions includes the ground state and various excited states. As it is not possible to include all the excited states in the solution of the Boltzmann equation, we consider a condition that each species includes the ground state and only a few low lying excited states (as mentioned above) which follow a Boltzmann distribution and have a global density equal to the equilibrium value. This procedure of parametrizing the concentration of these states equal to the given equilibrium value at a fixed gas temperature allows us to understand the role of excited states [40]-[41] although it might give some deviation from the actual species concentration.

It is worth to mention that the time scale of a single electron avalanche is usually short compared to the characteristic time of the neutral kinetics, and thus, the change of the neutral species concentration during the breakdown process can be neglected. Therefore, the equilibrium composition can be used for the calculation of the electrical breakdown, which is a typical non-equilibrium process with EEDF departing from the Maxwellian distribution. Under the equilibrium condition, it is assumed that the forward electron-ion recombination rate is balanced with the reverse reaction rate (i.e., for electron-ion pair formation) and the influence of electron-ion recombination is therefore not taken into account in the ions kinetics. Note that the equilibrium species composition is a rather exceptional case in reality. For example, when a hot gaseous mixture is produced by a rapid quenching of the plasma from an elevated temperature, the composition of the hot gas may depart from the equilibrium composition. Especially the charged species will be overpopulated because the ions and electrons have not enough time to recombine into neutral species, as dictated by the reaction rates. In order to account for the influence of this kind of ion overpopulation on the electron-ion recombination, we artificially increase the concentrations of the charged species by a factor two compared to the equilibrium concentrations (see text below).

Table 2 Overview of the vibrational and electronically excited levels of molecular species CO_2, CO andO_2 included in the model.

Species	Notation	Excited state(s)	Energy level (eV)
CO_2	CO_2v1	(0 1 0)	0.083
	CO_2v2	(0 2 0) + (1 0 0)	0.167
	CO_2v3	(0 30) + (1 1 0)	0.252
	CO_2v4	(0 n 0) + (n 0 0) [(a)]	0.339
	CO_2v5	(0 n 0) + (n 0 0) [(a)]	0.442
	CO_2v6	(0 n 0) + (n 0 0) [(a)]	0.505
	CO_2v7	(0 n 0) + (n 0 0) [(a)]	2.500
	CO_2v8	(0 0 1)	0.291
	CO_2e1 [(b)]		10.50
CO	COv1	$n_v = 1$	0.266
	COv2	$n_v = 2$	0.528
	COv3	$n_v = 3$	0.787
	COv4	$n_v = 4$	1.040
	COv5	$n_v = 5$	1.300
	COv6	$n_v = 6$	1.540
	COv7	$n_v = 7$	1.790
	COv8	$n_v = 8$	2.030
	COv9	nv = 9	2.270
	COv10	nv = 10	2.510
	COe1	$A^3\Pi$	6.220
	COe2	$A'\ ^3\Sigma$	6.800
	COe3	$A^1\Pi$	7.900
	COe4	$b^3\Sigma$	10.400
	COe5	$C^1\Sigma$ + $E^1\Pi$	10.600

O_2	O_2v1	$n_v = 1$	0.190
	O_2v2	$n_v = 2$	0.380
	O_2v3	$n_v = 3$	0.570
	O_2v4	$n_v = 4$	0.750
	O_2e1	$a^1\Delta_g$	0.977
	O_2e2	$b1\Sigma g^+$	1.627
	O_2e3	$A^3\Sigma u^+$ + $C^3\Delta u$ + $c^1\Sigma u^-$	4.500
	O_2e4	$B^3\Sigma u^-$	8.400
	O_2e5 [c]		9.970

(a) A generic notation "n" for the levels CO_2v4-v7 is used, as they are composed of several individual levels.

(b) The exact notation of the electronically excited level CO_2e1 is not known (see ref [42]).

(c) The exact notation of the electronically excited level O_2e5 is not known (see ref [43]).

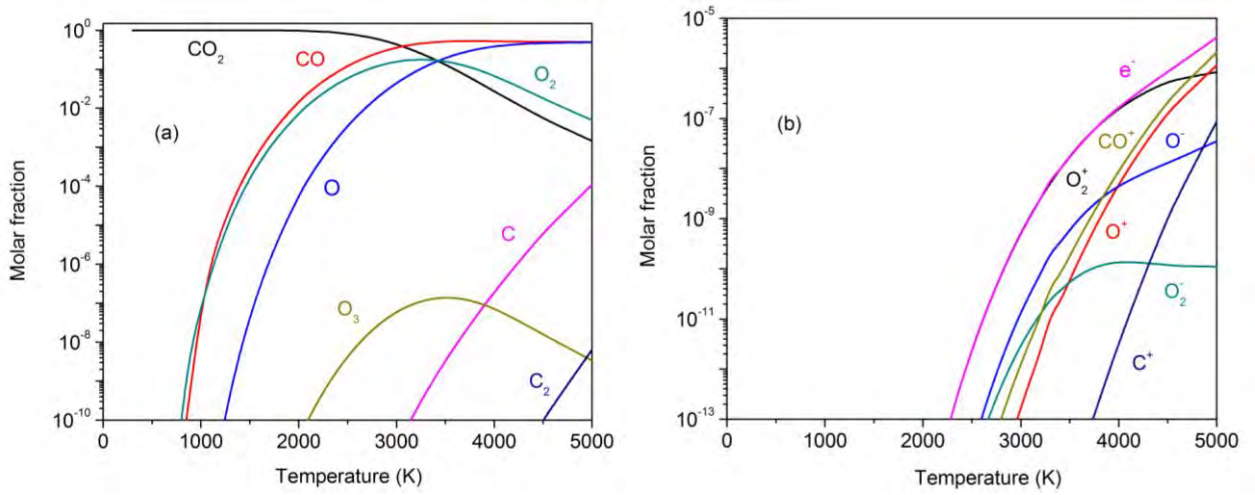

Fig.1 Calculated species composition of CO_2 and its dissociation products (a), as well as the corresponding charged particles (b), as a function of gas temperature at atmospheric pressure. The sum of ground state and all vibrational and electronically excited levels is plotted for each neutral species. Only the most important species are plotted; the ions with negligible densities under the equilibrium conditions are not presented here.

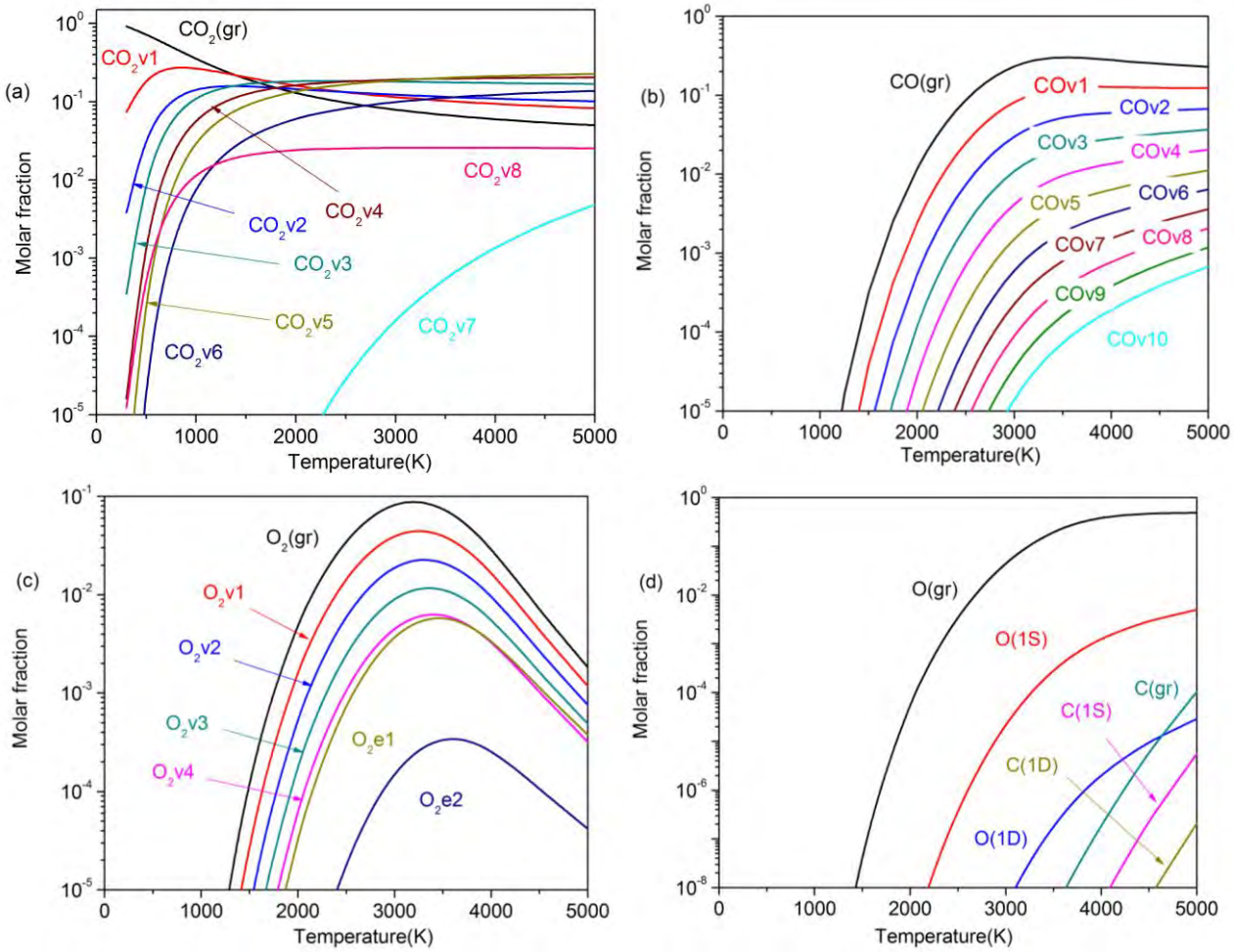

Fig.2 Calculated molar fraction of the ground state and the various vibrational and electronic states of CO_2 (a), CO (b), O_2 (c), and O and C (d), as a function of gas temperature at atmospheric pressure. For CO_2 and CO, only the vibrational states are presented, because the electronically excited states have a negligible molar fraction. For O_2, only the two lowest electronically excited states are shown, besides the vibrational levels, for the same reason.

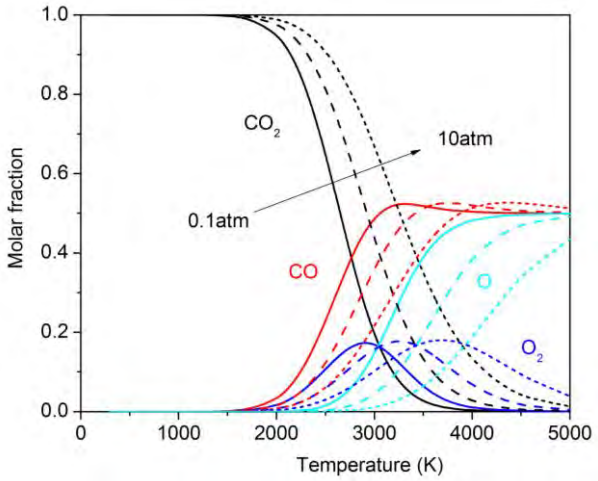

Fig.3 Calculated CO_2, CO, O and O_2 molar fractions as a function of gas temperature, at a pressure of 0.1 atm (solid lines), 1 atm (dashed lines) and 10 atm (short dashed lines).

Fig.1 shows the calculated molar fractions of CO_2 and its dissociation (and ionization) products as a function of temperature in the range from 300 K to 5000 K at atmospheric pressure. Above around 2000 K, CO_2 starts to dissociate into CO and O_2. A further temperature increase above 3000 K promotes the dissociation of O_2 into O atoms. Because the dissociation products of CO_2, i.e. CO, O_2 and O, have different electron kinetics, this might influence the effective ionization coefficients and hence change the critical reduced breakdown electric field strength of the gas mixture. The ions are generated above 3500K and their concentration increases with rising temperature. Only the dominant ions are plotted in Fig. 1(b); the other ions have negligible densities under the equilibrium conditions. The electron fraction is also plotted, and is obtained from the molar fractions of the various positive and negative ions, based on electrical charge neutrality.

Assuming a Boltzmann distribution with an excitation temperature identical to the gas temperature, we can obtain the molar fractions of the various vibrationally and electronically excited states, as is presented in Fig. 2 for CO_2, CO, O_2, O and C (except for the electronically excited states of CO_2 and CO and the highest electronically excited states of O_2, which have negligible molar fractions). With increasing gas temperature, the concentration of the CO_2 vibrational levels can even exceed that of the ground state (see Fig. 2(a)). Therefore, the electron kinetics of the excited species might also influence the effective ionization coefficients of the gas mixture and thus the critical reduced breakdown electric field strength at elevated temperature.

Finally, Fig. 3 shows the calculated molar fractions of CO_2, CO, O and O_2 at a pressure of 0.1 atm, 1 atm and 10 atm, again in the temperature range from 300K to 5000K. The dissociation of CO_2 and thus also the concentration of its dissociation products is shifted to higher temperature with increasing pressure.

From these figures, we can conclude that the gas temperature and pressure can significantly affect the concentrations of the dissociation products and of the various excited states and ionic species. Therefore, the electron interactions with these species, as well as the ion kinetics, must be taken into account when calculating the effective ionization coefficients and the critical reduced breakdown electric field strength, which will be discussed in detail in the following sections.

3. Electron-gas collision cross sections and ion kinetics

3.1 Electron-gas collision cross sections

For determining the critical breakdown electric field, we need to calculate the rates of electron production and loss, which are determined from the electron impact ionization, electron attachment and detachment, and electron-ion recombination coefficients. Thus, we need to calculate the electron energy distribution functions (EEDFs), based on the cross sections of all relevant processes. We take into account here the interaction of electrons with the ground state and various excited states of the following neutral

species: CO_2、CO、O_2、O and C, as well as with the ground state of O_3 and C_2. Not all cross section data, especially for the interaction between electrons and excited species, are available in the literature. The electron-impact momentum transfer, excitation, ionization and attachment cross sections for the interactions between electrons and the ground states species are adopted from standard databases (see below and Appendix 1).

As explained in previous section, we take into account a simplified CO_2 energy ladder, describing the excitation from the ground state v0 (000) to eight vibrational levels, including the first bending mode level v1 (010), the first asymmetric stretching mode level v8 (001), and 6 mixing levels (Fermi resonance levels) v2-v7 (0n0+n00), as well as one electronic level (e1) with threshold energy at 10.5 eV. The other important electronic level with threshold energy at 7.0 eV is considered as dissociative channel, but electron impact excitation from the ground state to this electronically excited level is of course also included. This treatment is in agreement with those one by Pietanza et al. [35]-[36] although recently Pietanza et al [46] have developed a updated database, which substitutes the above mentioned dissociation with the experimental data by Cosby and Helm [47]. The relevant cross sections are taken from the database of Phelps and coworkers [42],[44], supplemented by the dissociative ionization channels recommended by Itikawa [45].

The cross sections for the electron interactions with the ground state of the other neutral species, CO, O_2, O_3、C_2、O and C are based on reference [43],[48]-[58]. The detailed reaction set for the electron interactions with neutral species, as well as the references where the cross section data are adopted from, is tabulated in table 3 in the Appendix. Calculations show a strong dependence of dissociative attachment on the vibrational quantum number for molecular oxygen [59]. Therefore, we include the most recent cross section sets calculated by Laporta et al.[49],[53] for the dissociative electron attachment with the vibrationally excited states of CO and O_2. It is found that the dissociative electron attachment cross section of vibrationally excited molecules of CO and O_2 increases rapidly with the increasing of vibrational quantum number. This can influence the electron attachment rate and hence the critical reduced breakdown electric field (see section 5.3). The ionization cross sections of vibrationally excited O_2 molecules, which are available via the website of the Phys4Entry project [60], are from the calculation of Kosarim et al.[52]. Kosarim et al.[52] also performed a calculation of the ionization cross section of electronically excited O_2 molecules, however, the full data set is not available to us. Therefore, for the electronically excited states O_2e1 ($O_2(a1\Delta g)$) and O_2e2 (O_2 ($b1\Sigma g^+$)), the ionization cross sections are approximated by a threshold shift following a similar treatment as in reference [61]. Our calculation shows that for the cases considered in this work, the role of the electronically excited states of molecular species is minor in the ionization process due to their quite small concentrations. For the ionization of electronically excited O atoms, we take into account the cross section set evaluated by Pandya et al. [62].

The interaction cross sections between electrons and the other excited species are not completely available in the literature and different approximation methods were used in literature to evaluate the influence of excited states on the electron kinetics [63]-[65]. One approach is to assume that all the vibrational states may

be ionized and excited with a cross section identical to that for ionization and excitation from the ground state [50]. On the other hand, some scaling laws can also be used to estimate the cross section sets of excited states [64]-[65]. In our work, the electron impact excitation cross sections σ_{nm} for excitation from $CO_2v(n)$ to $CO_2v(m)$ at each vibrational mode (i.e., n = 1-6; m = 2-7) were obtained by the Fridman approximation [64] from the known cross section σ_{01} for excitation from the ground state to the first vibrational state:

$$\sigma_{nm}(\varepsilon) = \frac{\exp(-\alpha(m-n-1)}{1+\beta n}\sigma_{01}(\varepsilon + E_{01} - E_{nm}) \tag{4}$$

where $E_{01} = E_1 - E_0$ and $E_{nm} = E_m - E_n$ are the corresponding excitation threshold energies. Thus, the Fridman approximation shifts the cross sections on the energy scale to account for the change in the threshold energy and it scales the magnitude of the cross sections according to two parameters, α and β. For CO_2, we use α = 0.5 and $\beta = 0$ as suggested in [64], i.e. the cross section σ_{12} has the same magnitude as σ_{01}. This approach is a kind of semi-empirical approximation for multi-quantum vibrational excitation. The parameters chosen here yield good agreement with experimental work [44] for the cross section data of electron impact excitation to the lower asymmetric mode vibrational levels.

The vibrational cross section sets for electron impact excitation from the lower to higher vibrational states of CO and O_2 are obtained by a similar scaling and shifting using Fridman's approximation. For inter-mode vibrational excitations of $CO_2v(n)$ to $CO_2v(m)$ (i.e., n = 1-7; m = 8 or n = 8; m = 1-7), we assume that these processes have the same cross section value as from the ground state.

For the elastic collisions, we assume that the interactions between electrons and excited species have the same cross sections as for the ground states. Similarly, electron impact ionization of the vibrational levels and excitation from (vibrationally or electronically) excited states to other electronically excited states is likely to proceed to another vibrationally excited state of the correspond ion or excited molecule (according to the Frank–Condon principle) and thus we assume no effect of the vibrational energy on these types of reactions, i.e., the same cross sections as for the ground state reactions are used. In contrast, as vibrational excitation is most effective in lowering the energy barrier for dissociation and dissociative ionization and attachment reactions, the threshold energy of the cross sections for these processes is lowered by the vibrational energy of the levels. Finally, for electron impact excitation and ionization of an excited atomic level, we also utilize the cross sections of the ground state and again shift the energy dependence by the energy of the excited level.

By means of these approaches to estimate the missing cross sections for interactions between electrons and excited species, we can investigate the influence of the excited states on the electron impact ionization and attachment kinetics and hence on the critical reduced breakdown electric field strength. We should stress that the accuracy of the calculated breakdown electric field strength largely depends on the used cross section set. Although we tried to include the most reliable cross sections derived by reproducing the experimental

swarm transport properties through a Boltzmann analysis or theoretical calculation, the present results might still be subject to improvement, because some approximations are used in the establishment of the electron impact cross sections with the vibrationally and electronically excited states. In order to develop an improved database, experimental work is of great significance to help validate the theoretical evaluation.

3.2 Ion kinetics

The critical breakdown electric field will be higher when the electron avalanche is limited, by removing electrons, e.g., due to electron-positive ion recombination or electron attachment, while it will be lower when the electron avalanche is enhanced, e.g., by ionization or electron detachment from negative ions. Thus, the ion kinetics must be taken into account [27]. Therefore, the ion kinetics including electron-ion recombination, electron detachment from these negative ions, charge transfer reaction, as well as ion clustering reactions, which also play an important role as electron kinetics in electrons production and loss, should be taken into account in the evaluation of hot gas breakdown.

The electron-ion recombination reactions gradually become more important at elevated temperature, because of the higher ionization degrees (cf. Figure 1 above). The rate coefficients of the electron-ion recombination reactions are listed in table 4 in Appendix 2, and their backward rate coefficients (i.e., for electron-ion pair formation) are computed by the detailed balance principle based on an equilibrium constant defined by the partition functions of the reactants and reaction products.

It is known that a plasma in gas mixtures containing electronegative gases (i.e., from which negative ions are readily produced) often exhibits markedly different behavior from a plasma in electropositive gases [66]. In the gas mixture of CO_2 and its dissociation products, electron attachment reactions with CO_2 and atomic oxygen produce O^- ions, while electron attachment with O_2 and O_3 produce either O^- or O_2^- ions (see table 3 in Appendix 1). The electron attachment with CO is quite weak and therefore ignored in our work.

Vice versa, the (associative) detachment of electrons from O^- and O_2^-, mainly upon reaction with CO, O_2, O_3 or O, which are the dominant dissociation products of CO_2, has a high reaction rate coefficient (depending on the collision partner; see table 4 in Appendix 2) and can thus influence the breakdown behavior at sufficiently high concentrations of these species. This process turns out to be especially important for CO, due to its relatively high concentration (see Figure 1).

Finally, clustering of the O^- ions with either CO_2 or O_2 will lead to the formation of CO_3^- or O_3^-, which are stable negative ions. This process is especially important for the formation of CO_3^-, due to the high concentration of CO_2. The destruction of this cluster ion is more difficult due to its high electron affinity and/or the greater cluster bond energy [66]. In addition, this clustering reaction occurs at a time scale which is much faster than for typical electron detachment reactions. Thus, three-body clustering reactions can very

rapidly convert the initial negative ions (*i.e.,* mainly O^-) to more stable cluster ions at high enough CO_2 concentrations. Therefore, the two ion reactions mentioned above, i.e. associative detachment and cluster stabilization, compete with each other as destruction channels for O^-, to produce either new electrons or stable CO_3^- cluster ions, respectively. To complete the ion kinetics in our model, one more ion reaction is included, i.e., ion conversion from O_2^- to O^- (see table 4 in Appendix 2).

In the low temperature range, when the dissociation of CO_2 is weak, the concentration of CO, which is mainly responsible for the detachment reactions, is low, and hence the effective detachment rate is low. In this case, the influence of detachment processes on the electron formation and hence on the effective ionization coefficients is quite limited, while cluster stabilization plays an important role in the conversion of the negative ions O^- (generated by electron attachment) into stable cluster ions. Thus, the balance of electron generation and loss is mainly controlled by electron impact ionization and electron (dissociative) attachment of (mainly) CO_2.

However, when the gas temperature increases, the dissociation degree of CO_2 gradually increases as well, and the reaction rate of cluster ion formation decreases. At the same time, the destruction rate of the negative ions O^- upon collision with CO, leading to electron detachment, will increase. At a certain gas temperature, the concentration of CO is sufficiently high, so that the electron detachment reaction upon collision with CO can effectively compete with the ion cluster formation. In this case, the negative ions (mainly O^-) produced by electron (dissociative) attachment can almost instantaneously be lost by associative electron detachment. Thus, the net contribution of electron (dissociative) attachment on the electron loss will become zero and the balance of electron generation and loss will be mainly controlled by electron impact ionization and electron-ion recombination. These considerations stress the importance of including the ion kinetics when calculating the effective ionization coefficients and the critical reduced breakdown electric field from the balance between electron production and loss.

The above mentioned ion kinetics, and their effect on the electron production and loss, is schematically summarized in the following diagram. The electron attachment and detachment reactions are indicated with blue and red arrows, respectively, while the ion cluster reactions of O^- and the charge transfer reaction from O_2^- to O^- are presented with green and pink arrows respectively. Finally, recombination and ionization are just written in black.

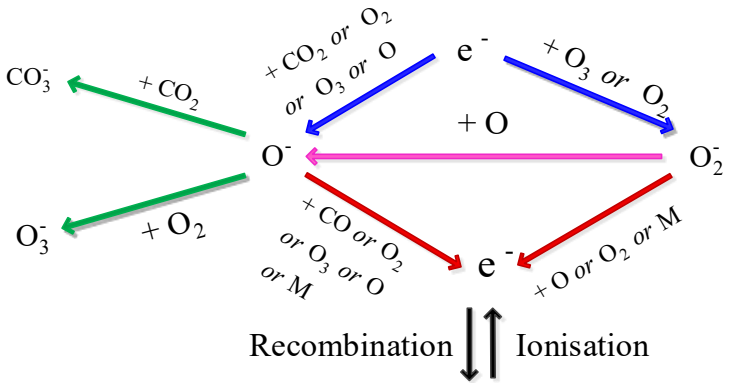

4. Determination of the effective ionization coefficients and the critical reduced breakdown electric field strength

In our work, we take into account both the electrons and ion kinetics described in previous section, and we apply a similar theoretical model as proposed by Verhaart and van der Laan [67]. Four different species are involved in the determination of the effective ionization coefficient: electrons (e^-), positive ions (p), unstable negative ions (nu) and stable negative ions (ns). The stable negative ions in our case are O_3^- and CO_3^-, while the unstable negative ions are O^- and O_2^-. The latter have a relatively short lifetime and are able to either release their electron (i.e., electron detachment), or to be converted into stable ions (including the charge transfer reaction from O_2^- to O^-, which is then further converted into stable ions) within the ion transit time. The development of an avalanche of electrons, unstable and stable negative ions and positive ions can thus be expressed as

$$\frac{\partial N_e}{\partial x} = \alpha N_e - \eta N_e + \delta N_{nu} - \gamma N_e \tag{5}$$

$$\frac{\partial N_{nu}}{\partial x} = \eta N_e - \delta N_{nu} - w N_{nu} \tag{6}$$

$$\frac{\partial N_{ns}}{\partial x} = w N_{nu} \tag{7}$$

$$\frac{\partial N_{np}}{\partial x} = \alpha N_e - \gamma N_e \tag{8}$$

where α, η, γ, δ, ω are the Townsend coefficients of electron impact ionization, electron attachment, electron-ion recombination, electron detachment and conversion of unstable to stable negative ions, respectively. They are again expressed in m^{-1}, and they represent the number of "events" of the above processes, per unit length and normalized per electron. Considering that the electrons have a much higher drift velocity than the positive ions, we can ignore the drift of positive ions during the electron avalanche development, which has a quite short time scale, in the evaluation of the electron-ion recombination rate.

To determine the effective ionization coefficient α_{eff}, we solve this system of equations, and express the electron avalanche in the following form:

$$N_e = N_e^0 \exp(\alpha_{eff} x) \tag{9}$$

Substituting the latter into the above system of equations and limiting ourselves to the solution of $\alpha_{eff} > 0$ [68], we obtain the following expression for the effective ionization coefficient (See Supporting Information):

$$\alpha_{eff} = (\alpha - \eta - \delta - \omega - \gamma) + \sqrt{(\alpha - \eta - \delta - \omega - \gamma)^2 + 4\ (\alpha - \gamma)\delta + (\alpha - \eta - \gamma)\omega}\ \ / 2 \tag{10}$$

When electron-ion recombination is ignored, this expression reduces to equation (11), which was derived in [67] and [68].

$$\alpha_{eff} = (\alpha - \eta - \delta - \omega) + \sqrt{(\alpha - \eta - \delta - \omega)^2 + 4\ \alpha\delta + (\alpha - \eta)\omega}\ \ / 2 \tag{11}$$

Under the condition that electron-ion recombination is weak (γ=0), it is easy to check that $\alpha-\eta \le \alpha_{eff} \le \alpha$ (See Supporting Information).

In order to clarify the influence of the ion kinetics on the effective ionization coefficients and on the critical breakdown electric field, we will perform calculations using as initial value two different concentrations of all charged particles appearing in the system as we mentioned above. The first one is the equilibrium species composition at each gas temperature, as depicted in Figure 1 above and it is assumed that the forward recombination rate is balanced with the reverse reaction rate (i.e., for electron-ion pair formation). This is the same treatment as in ref. [67]-[68]. The other set of calculations is performed with an overpopulated ion composition by artificially increasing their concentrations by a factor two compared to the equilibrium concentrations. Note that these differences only influence the electron-ion recombination coefficient γ and will not change the other Townsend coefficients α, η, δ, ω. Therefore, unless mentioned otherwise, the results in the following sections related to these Townsend coefficients will be obtained using the equilibrium species composition as input. This corresponds to a condition that the electron-ion recombination processes are ignored (γ=0) for ions overpopulation condition.

The critical reduced breakdown electric field $(E/N)_{cr}$ corresponding to a zero effective ionization coefficient ($\alpha_{eff}\ \ E/N\ _{cr} = 0$), is defined by the following formula (See Supporting Information):

$$(\alpha - \gamma)\delta + (\alpha - \eta - \gamma)\omega = 0 \tag{12}$$

Equation (12) can be reduced to $\alpha - \eta - \gamma = 0$ when the electron detachment processes are negligible ($\delta = 0$), and it can be reduced to $\alpha - \gamma = 0$, when electron attachment is negligible ($\eta = 0$), or in other words, when electron detachment is very important so that it effectively compensates for electron attachment, and the net loss by electron attachment is zero.

If not specifically mentioned, equations (10) and (12) are used in the next section to determine the

effective ionization coefficients and the critical reduced breakdown electric fields.

The Townsend ionization and attachment coefficient are calculated from EEDF and the latter is obtained here from the Boltzmann transport equation, solved for a uniform, zero-dimensional space with the BOLSIG+ code [69]. It is known that electron–electron collisions cause the EEDF to tend towards a Maxwellian distribution function [69]**.** The influence of these collisions depends essentially on the ionization degree (n/N) and is known to become significant for n/N > 10^{-6}, which corresponds to about 5000 K at atmospheric pressure in our current work (see Figure 1). Therefore, we take into account the influence of electron–electron collisions in the solution of the Boltzmann transport equation, and the cross section is adopted from ref. [70].

5. Results and Discussion

5.1 Electron Energy Distribution Functions (*EEDFs*)

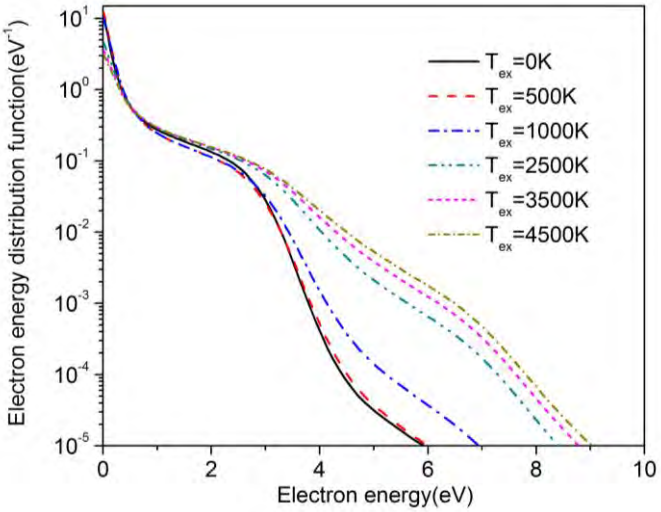

Fig.4 EEDFs calculated in pure CO_2 , i.e., at a temperature of 300K, when dissociation is negligible, at different vibrational excitation temperatures, and at atmospheric pressure and a reduced electric field of 25 Td, with vibrational kinetics treated with the Fridman approximation.

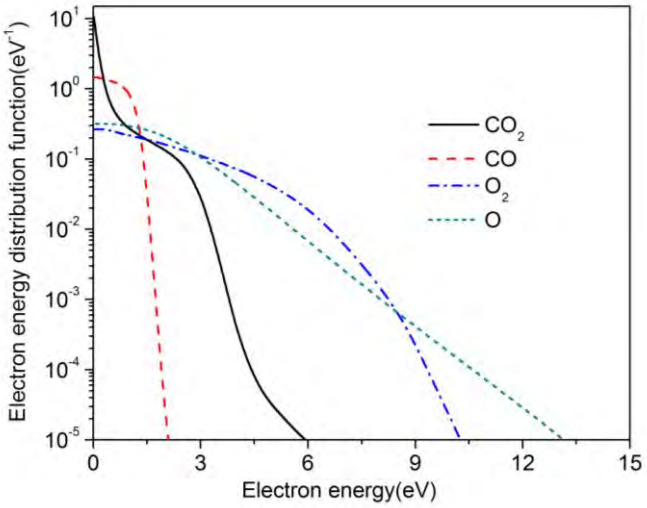

Fig.5 EEDFs calculated for pure CO_2, CO, O_2 and O at an excitation temperatures of T_{ex} = 0 K, a gas temperature of 300 K, atmospheric pressure and a reduced electric field of 25 Td.

Fig.4 presents the EEDFs calculated for pure CO_2 with different vibrational excitation temperatures, at atmospheric pressure and 300 K, and a reduced electric field of 25 Td, using the Fridman approximation to estimate the cross sections for vibrational excitation from the vibrational levels. The term 'vibrational kinetics' refers to the electron impact vibrational excitation and de-excitation processes between different vibrational states which are treated as independent species. With increasing vibrational excitation temperature, the molar fraction of the vibrational states increases and thus the superelastic vibrational collisions become more important, and this increases the average electron kinetic energy. Indeed, in a superelastic collision, a low-energy electron collides with an excited species, resulting in loss of the internal energy, leading to de-excitation of the neutral species and an increase in the kinetic energy of the electron. Thus, the EEDF becomes broader with a gradually decreasing peak value at low energy.

These results do not yet take into account the influence of the dissociation reactions, because CO_2 dissociation is negligible below around 2500 K (see Fig. 1 above). At higher temperatures, CO_2 starts to dissociate, and the shape of the EEDF curve will be markedly changed, which is attributed to the change of species composition and the associated energy exchange processes. This can be observed from Fig.5, where the EEDFs of the dominant dissociation products, i.e., CO, O_2 and O, are presented, together with the EEDF of pure CO_2. Compared with the EEDF of CO_2, the EEDF of CO is much more narrow, corresponding to a lower average electron energy, while O_2 and O yield a much broader EEDF under the same conditions. This is the direct result of different electron energy loss processes with these different species. Therefore, we can conclude that for temperatures above 2500 K, when CO_2 splitting starts to become important, the gas temperature will influence the dissociation products and hence this will affect the overall shape of the EEDF.

The latter is indeed observed from Fig.6, showing the influence of the gas temperature, as well as of the reduced electric field strength, on the EEDFs in (partially dissociated) CO_2 at atmospheric pressure. Note that three different approaches are used to calculate the EEDFs, i.e., (1) neglecting the role of the vibrationally and electronically excited states, (2) including the vibrational levels but treating them with the same cross sections as for the ground states, and (3) including the vibrational levels and treating them with modified cross sections, as described by the Fridman approximation (see section 3.1 above). Note that in case 2 and 3, the electronically excited levels of the molecules and atoms are also included, following the treatment described in Section 3.1, but their effect is minor when the excitation temperature is equal to the gas temperature. However, they might become important at higher electronic excitation temperature, as will be illustrated below (see Fig. 7 below).

By comparing the EEDFs at 2500 K with those at 3500 K and 4500 K, we see a large deviation of the shape due to the gradually more significant role of the dissociation products (mainly CO; see Fig. 1 above),

making the EEDF more narrow. This is most apparent at E/N = 25 Td, when neglecting the effect of the vibrationally excited levels.

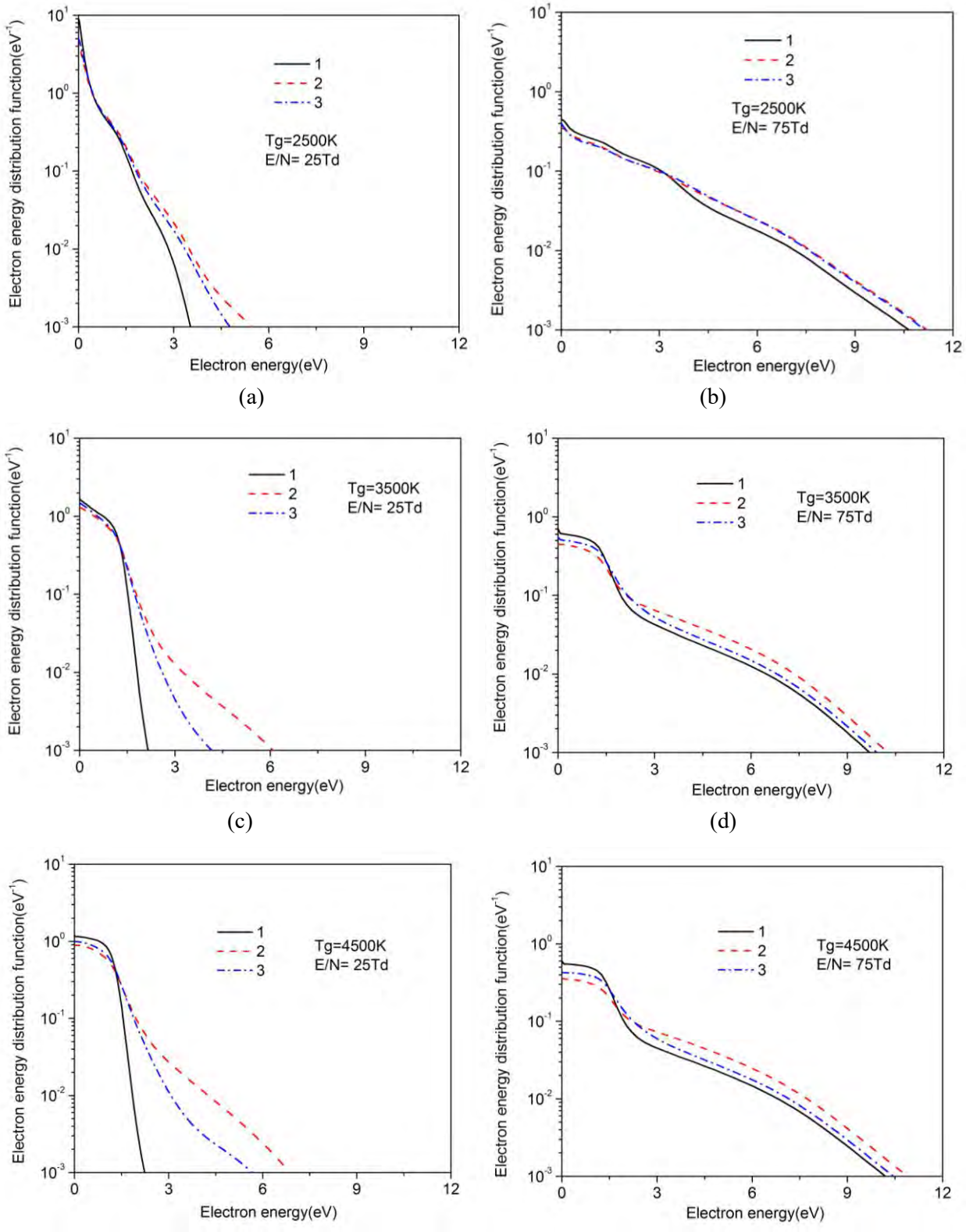

Fig.6 EEDFs calculated in CO_2 (and its mixture of dissociation products) at a gas temperature of 2500 K, 3500 K and 4500 K, at atmospheric pressure, and reduced electric fields of 25 Td and 75 Td. (1) Neglecting

the role of vibrationally and electronically excited levels of all species; (2) Including vibrational levels but treating them with the same cross sections as for the ground state (so-called ground state approximation); (3) Including vibrational levels and treating them with modified cross sections, as obtained from the Fridman approximation (see section 3.1). Electronically excited levels of the various molecules and atoms are also included in cases (2) and (3), but are of minor important in this case; see text below. The excitation temperature for all species is equal to the gas temperature.

With increasing reduced electric field at a fixed gas temperature, the fraction of electrons with higher energy drastically increases, which is logical because the electrons are more accelerated by the electric field. Similarly, the vibrationally excited states greatly affect the EEDF, especially at low E/N (left figures) and high gas temperature, which is obvious when comparing in each figure curves 2 and 3 with curve 1, obtained when neglecting the excited states. Indeed, when considering the vibrationally excited states, the fraction of electrons with higher energy increases as a result of the contribution of superelastic collisions, as was also clear from Fig. 4, and from [34]-[36]. At higher E/N (right figures), the deviation between the EEDFs calculated when neglecting the vibrational levels and when including them, assuming either the same cross sections as for the ground state or the Fridman approximation, is much lower. The reason is that the fraction of energy consumed by the vibrational excitation channels, which have a relatively low energy threshold, is decreasing, while the fraction of energy loss due to electronic excitation and ionization is increasing. Furthermore, in all cases, the EEDFs calculated when considering the same cross sections for the vibrational levels as for the ground states (i.e., curves 2, in red) are somewhat broader than when assuming the Fridman approximation (i.e., curves 3, in blue). Indeed, the former does not take into account the shift in threshold energy and hence underestimates the vibrational excitation rates and the corresponding energy losses. Note that the curves 1 (in black) neglect the vibrationally and electronically excited levels, and thus the superelastic collisions (leading to broadening of the EEDF), but they still account for excitation to these levels, leading to energy loss, the same as for the curves 2 and 3.

In summary, Fig. 6 clearly illustrates the importance of including the vibrational levels, with the more realistic cross sections as obtained from the Fridman approximation, especially at low E/N values, as well as including the CO_2 dissociation products, especially at higher gas temperatures, for an accurate calculation of the EEDF.

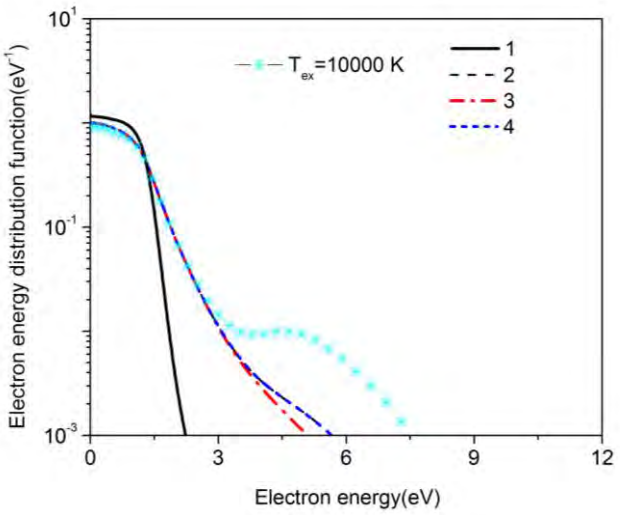

Fig.7 EEDFs calculated in CO_2 (and its mixture of dissociation products), at a gas temperature of 4500 K, at atmospheric pressure and a reduced electric field of 25 Td. (1) Neglecting the role of vibrationally and electronically excited levels of all species; (2) Including vibrationally and electronically excited levels of all species using the Fridman approximation, and T_{ex}=T_{gas}; (3) Neglecting electronically excited levels of atomic species (C and O) , and T_{ex}=T_{gas}; (4) Neglecting electronically excited levels of molecular species (CO_2, CO and O_2), and T_{ex}=T_{gas}. The EEDF calculated with an electronic excitation temperature T_{ex}=10,000K (see text) for both the atomic species and molecular species is also presented for comparison (see cyan symbols), while the vibrational excitation temperature is still equal to the gas temperature.

To illustrate the influence of the electronically excited levels on the EEDF, we compare in Fig. 7 the EEDFs calculated when neglecting both the vibrationally and electronically excited levels, with the case when including both levels, as well as with the case when the vibrationally excited levels are included, but either the electronically excited levels of the molecules or of the atoms are neglected. The energy levels of the vibrationally excited species start at energies of 0.083 eV for CO_2, 0.266 eV for CO, and 0.190 eV for O_2; see Table 2 above. Furthermore, the electronically excited levels of the C and O atoms and of the O_2 molecules are also at relatively low energies (i.e., starting at 1.26 eV and 1.97 eV for C and O, and at 0.977 eV for O_2), while the electronically excited levels of CO_2 and CO start at 10.5 eV and 6.22 eV, respectively (not taking into account the 7 eV level of CO_2, which is treated as dissociative level). The electronically excited levels are also assumed to follow a Boltzmann distribution, with the excitation temperature assumed to be equal to the gas temperature, i.e. T_{ex}=T_{ga}.

Our calculations predict that superelastic collisions of the excited C and O atoms, in addition to those considered for the vibrationally excited molecules, result in a slightly larger population of high-energy electrons at higher gas temperature above around 4000 K. This is depicted in Fig. 7. Indeed, when assuming T_{ex}=T_{ga}, the EEDF presented by curve (3), which corresponds to the case when the vibrationally and electronically excited levels of the molecules are included, but the electronically excited levels of the atoms are neglected, is slightly narrower than the EEDF presented by curve (2), which includes all vibrationally and

electronically excited levels, and the latter coincides with curve (4), which only neglects the electronically excited levels of the molecules. Thus, Fig. 7 illustrates that the electronically excited levels of the molecules have a negligible effect on the EEDF, while the electronically excited levels of the atoms have some effect, but the major effect in broadening the EEDF is due to the vibrational levels, under the condition that the excitation temperature is equal to the gas temperature.

On the other hand, it is well possible that the electronic excitation temperature reaches a higher value than the gas temperature [79]-[80], for example in case of a strong electric field, which yields a large electron impact excitation rate. Therefore, we also present in Fig. 7 the influence of a higher electronic excitation temperature (T_{ex}=10,000K) for both the atoms and molecules on the EEDF (cyan symbols). A significant deviation can be observed when comparing this curve with the EEDF obtained using an electronic excitation temperature equal to the gas temperature (i.e., curve 2). The much broader EEDF is again attributed to the important role of electronic superelastic collisions, especially for the atomic species, as their concentration is higher than those of the electronically excited molecules at a gas temperature of 4500 K.

5.2 Effective ionization coefficient

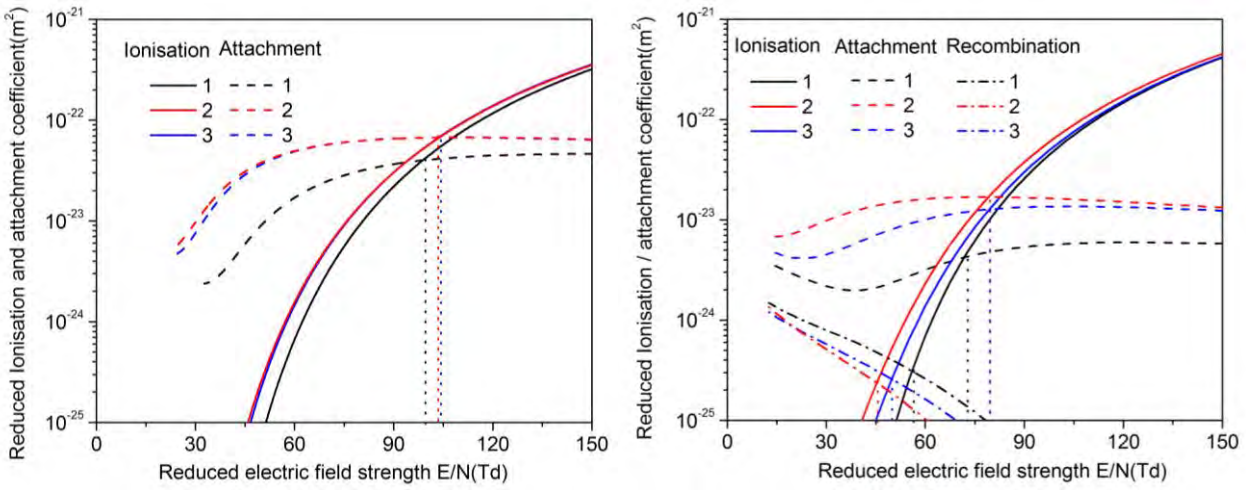

Fig.8 Reduced ionization coefficient (α/N; solid lines) and attachment coefficient (η/N; dashed lines) of CO_2 (and its mixture of dissociation products), as a function of reduced electric field strength at a gas temperature of 2500 K (a) and 4500 K (b) and atmospheric pressure. (1) Neglecting the role of vibrationally and electronically excited levels of all species; (2) Vibrational kinetics with ground state approximation; (3) Vibrational kinetics with Fridman approximation. The critical reduced electric field strengths at which the curves of the reduced ionization coefficients cross the curves of the reduced attachment coefficients (i.e., considering only the electron kinetics) are also indicated with vertical dotted lines. In figure (b), the reduced electron-ion recombination rate coefficient using an overpopulated ion composition (see text) is also presented for comparison (see dash-dotted lines), and likewise, the critical reduced electric field strengths at which the curves of the reduced ionization coefficients cross the curves of the reduced recombination coefficients (i.e.,

considering also the ion kinetics; see text) are also indicated with vertical dotted lines. The excitation temperature for all species is assumed equal to the gas temperature.

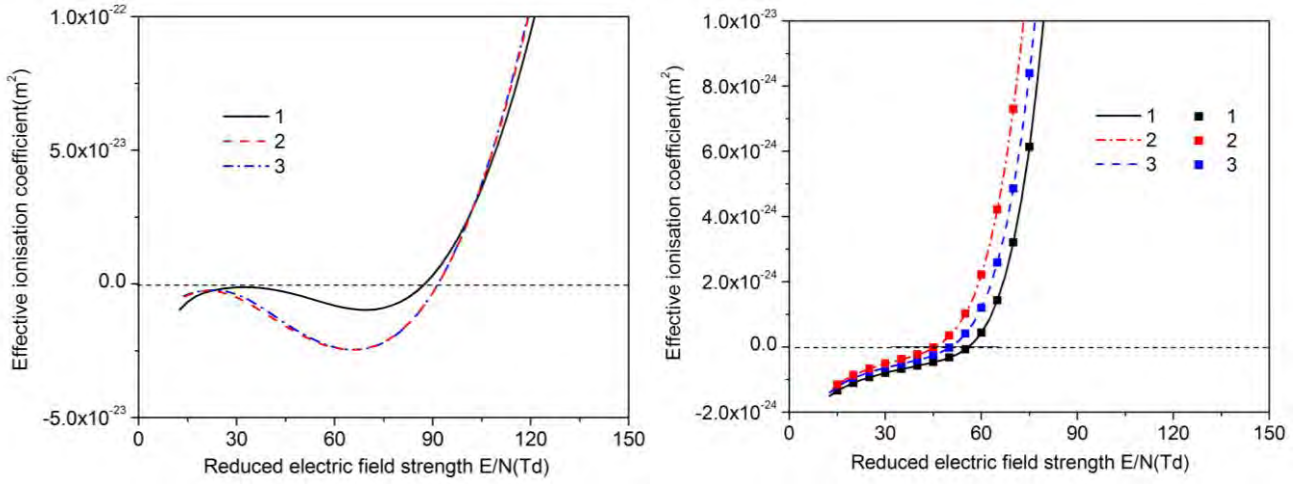

(a) (b)

Fig.9 Effective reduced ionization coefficient (α_{eff}/N) of CO_2 (and its mixture of dissociation products), defined by formula (10), as a function of reduced electric field strength at a gas temperature of 2500 K (a) and 4500 K (b) and atmospheric pressure. (1) Neglecting the role of vibrationally and electronically excited levels of all species; (2) Vibrational kinetics with ground state approximation; (3) Vibrational kinetics with Fridman approximation. The effective reduced ionization coefficient considering simply the balance between ionization and recombination using an overpopulated ion composition, instead of calculating it with formula (10), is also presented with symbols in figure 9(b).

In literature, the effective ionization coefficient is typically obtained by balancing the ionization and attachment coefficient, thus neglecting the role of the ion kinetics [25]-[33]. In this section, we investigate how the ion kinetics affect the effective ionization coefficient, as calculated with formula (10) above, compared to the simple balancing between ionization and attachment coefficients, besides studying the effect of including the vibrational levels.

To evaluate the difference between the effective ionization coefficient including the ion kinetics and the simple balancing between ionization and attachment coefficient, we plot in Figure 8 the variation of the reduced ionization and attachment coefficients, as a function of reduced electric field at a gas temperature of 2500 K and 4500 K and atmospheric pressure, with and without including vibrational excitation, i.e., the same approximations as used in Fig. 6. In Fig. 8(b), also the reduced electron-ion recombination coefficient is shown, considering an overpopulated ion composition by artificially increasing the ion concentration by a factor 2. The latter is done because an equilibrium ion composition would yield the same rate for electron-ion recombination as for the reverse process, i.e., electron-ion pair formation, so that there is no net effect of electron-ion recombination. This might happen when the plasma experiences very rapid quenching and the electrons and ions may not have enough time to recombine into neutral species. Under these conditions, the ion composition is larger than their equilibrium composition. These are the conditions we generally meet in a

circuit breaker [24],[81] and a gliding arc plasma [5] where the temperature cooling rate is often very high, i.e., up to 5×10^8 K s^{-1}. In this case, there will be a net effect of electron-ion recombination as electron loss mechanism. Below, we will discuss in more detail the difference between assuming an equilibrium ion composition vs an overpopulated ion composition.

The reason why we add the reduced electron-ion recombination coefficient to Fig. 8(b) is because at this high temperature (4500 K), the ions and the ion kinetics play a non-negligible role. As mentioned in section 4 above, depending on the exact ion kinetics, when electron detachment is more important than ion clustering, the electron attachment rate can be effectively balanced by the detachment rate from the negative ions, so that the main loss process for the electrons is electron-ion recombination. This represents one extreme situation of including the ion kinetics. The other extreme situation is when electron detachment is less important than ion clustering, so that the electron attachment rate is not balanced by the detachment rate, and in this case, electron attachment will be the main loss process for the electrons. This result also corresponds to the case when the ion kinetics are simply neglected. Thus, the curves for the reduced attachment coefficients and reduced electron-ion recombination coefficients in Fig. 8(b) represent the two extreme situations as electron loss mechanisms. Depending on the ion kinetics, the reality can also be a mix of both. Note that in Fig. 8(a) the curves for electron-ion recombination are not included, because this process plays a negligible role at 2500 K.

As discussed above, at a fixed gas temperature, considering the vibrational kinetics broadens the EEDF due to the effect of superelastic collisions of the vibrational levels, and this yields somewhat higher values of the reduced ionization and attachment coefficients, compared to the results obtained without vibrationally excited levels, especially at low reduced electric fields; see Fig. 8. As explained in Fig. 6, the ground state approximation underestimates the vibrational excitation rates and the corresponding electron energy losses. Therefore, this yields a somewhat broader EEDF and hence slightly overestimates the reduced ionization and attachment rate coefficients when compared with the results by the Fridman approximation, although the effect is minor.

It is clear from Fig. 8 that the reduced electron attachment coefficients increase more drastically than the reduced ionization coefficients when considering the vibrational kinetics, and thus the reduced electric field values at which the curves of the reduced ionization coefficients cross the curves of the reduced attachment coefficients become higher when considering the vibrational kinetics (see the vertical dotted lines in Fig. 8). Hence, the vibrational levels do affect the balance between ionization and attachment. This is attributed to the fact that the presence of vibrationally excited O_2 molecules increases the dissociative electron attachment more than the ionization upon rising vibrational quantum number.

In contrast, the electron-ion recombination coefficient, which is also plotted in Fig. 8(b), decreases when considering the vibrational states, due to an increased electron temperature as a result of the broader EEDF, and thus, the value of the critical reduced breakdown electric field strength, when it is determined by the

balance between ionization and recombination (see above), drops to lower values when including the vibrational levels (see the other vertical dotted lines in Fig. 8b, which indicate the position where the curves of ionization and recombination cross each other). This shows the importance of the vibrational levels in the determination of the reduced breakdown electric field strength when the ion kinetics is non-negligible, and when electron-ion recombination is important as electron loss process (see below).

Figure 9 shows the effect of the vibrational kinetics on the effective ionization coefficient, as calculated with formula (10), thus considering the entire ion kinetics, and using an overpopulated ion composition by artificially increasing the ion concentration by a factor 2 (see above, and see also further below). It is clear from comparing Fig. 9(a) with Fig. 8(a) that the effective ionization coefficient is not just the balance between ionization and attachment coefficients, because the position (i.e., reduced electric field value) where the latter curves cross (i.e., around 103.5 Td; indicated by the vertical dotted lines in Fig. 8(a)) does not coincide with the position where the effective ionization coefficient reaches zero (i.e., at about 91.5 Td). This is because electron detachment reduces the importance of electron attachment as electron loss mechanism, thus affecting the effective ionization coefficient.

Likewise, by comparing Fig. 9(b) with Fig. 8(b), it is clear that the effective ionization coefficient, as calculated with formula (10), is different from the simple balance between ionization and attachment, but it coincides quite well with the balance between ionization and recombination, as presented by the symbols in Fig. 9(b). This indicates that under these conditions the effective ionization coefficient, and thus also the critical reduced breakdown electric field, are determined by both the electron and ion kinetics, and that electron-ion recombination is the main electron loss mechanism.

Finally, it is clear from Fig. 9 that the vibrational kinetics do affect the effective ionization coefficient, when fully accounting for the ion kinetics. This is most apparent from Fig. 9(a), where curve 1 does not coincide with curves 2 and 3. The ground state or Fridman approximation for the vibrational kinetics, however, yields more or less the same results for the effective ionization coefficient (see curves 2 and 3). The reason why the vibrational kinetics affect the calculation of the effective ionization coefficient at 2500 K, in spite of the negligible role of electron-ion recombination, is due to the superelastic collisions which broaden the EEDF (see Fig. 6) and increase the ionization and attachment coefficients (see Fig. 8(a)), and thus also the difference between both. Moreover, the dissociative attachment cross section of vibrationally excited O_2 molecules increases more than the ionization cross section upon rising vibrational quantum number. This leads to an enhanced electron loss rate and therefore, the position at which the effective ionization coefficient becomes zero (i.e., where the ionization and attachment coefficients exactly balance each other), and thus the value of the critical reduced breakdown electric field is shifted to a higher value if the vibrational kinetics is taken into account (see also below). At 4500 K (Fig. 9(b)), the vibrational kinetics also affect the effective ionization coefficient, and in this case, there is a difference between the ground state and Fridman approximation as well.

Moreover, in this case, the position where the effective ionization coefficient reaches zero, and thus the value of the critical breakdown electric field, are also affected by the vibrational kinetics (see also below).

In the rest of this section, we will show the results obtained with vibrational kinetics included, according to the Fridman approximation. We will now investigate the effect of assuming an overpopulated ion composition on the effective ionization coefficient, and also compare the results with and without including the ion kinetics.

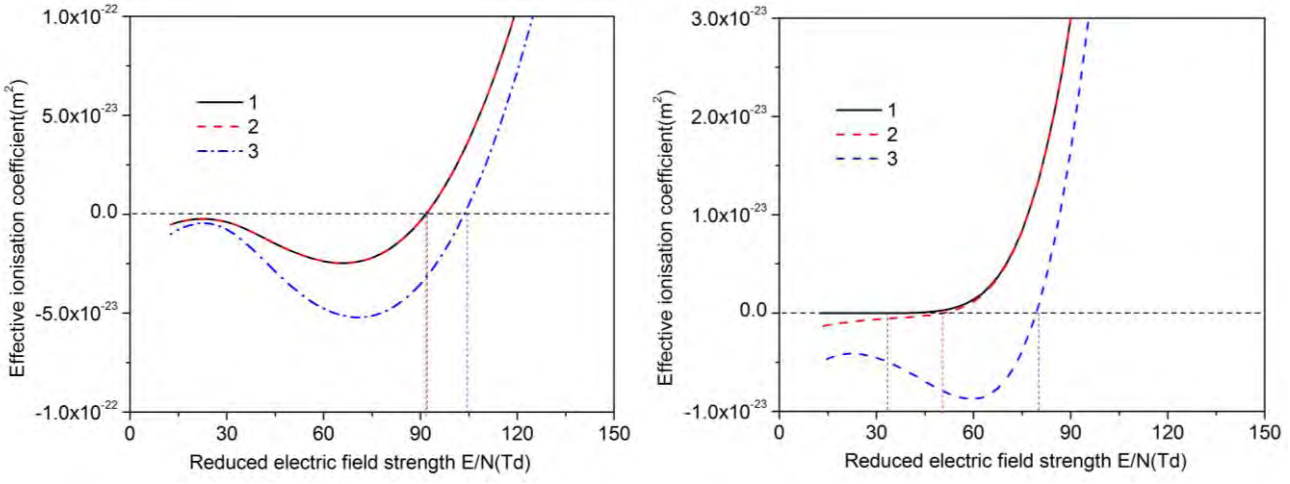

(a) (b)

Fig.10 Effective reduced ionization coefficient (α_{eff}/N) of CO_2 (and its mixture of dissociation products), as a function of reduced electric field strength at a gas temperature of 2500 K (a) and 4500 K (b) and atmospheric pressure, including the vibrational kinetics with the Fridman approximation. (1) Including ion kinetics with equilibrium composition; (2) Including ion kinetics based on an overpopulated ion composition; (3) Neglecting ion kinetics, so the effective reduced ionization coefficient is equal to the reduced ionization coefficient minus the reduced attachment coefficient ($(\alpha-\eta)/N$).

Fig.10 describes the influence of the ion kinetics, i.e., electron detachment and electron-ion recombination, on the effective reduced ionization coefficient as a function of reduced electric field, at a gas temperature of 2500 K (a) and 4500 K (b). At 2500K, both an equilibrium ion composition and an overpopulated ion composition (i.e., two times higher ion concentration) yield completely the same results for the effective reduced ionization coefficient (see Fig.10(a), curves 1 and 2). This is because the ion densities are very low and the reduced electron-ion recombination coefficient does not affect the loss of electrons. However, by comparing with curve 3, it is clear that, in spite of the low ion densities, the ion kinetics cannot be neglected. Indeed, curve 3 shows the effective ionization coefficient obtained from the simple balance of ionization and attachment. This balance yields clearly lower values for the effective ionization coefficient than when it is calculated with formula (10), and the corresponding critical reduced breakdown electric field, where the effective ionization coefficient is zero, is much higher. The reason is that in reality, when ion kinetics are included, the electron detachment from negative ions reduces the effective electron attachment rate, and thus

the loss of electrons, so that the effective ionization coefficient is higher, and the corresponding critical reduced breakdown electric field is lower.

With increasing gas temperature, the ion concentration increases and electron-ion recombination becomes more important in determining the effective ionization coefficient when the ion density is overpopulated, which indeed occurs quite often in non-equilibrium plasmas [24] , [81]. This can be seen by comparing the effective ionization coefficients in Fig. 10(b) at 4500K using an equilibrium ion composition (curve 1) and a (factor 2) overpopulated ion composition (curve 2). The equilibrium ion composition presented in Fig. 1 yields a balance between electron-ion recombination and the reverse process, i.e., electron-ion pair formation, as discussed in Section 4, and thus the net recombination rate hardly contributes to the electron loss. Thus, the effective ionization coefficient is slightly higher than when assuming an overpopulated ion composition. Again, when neglecting the ion kinetics, the results are completely different (see curve 3), because the effective ionization coefficient is simply obtained from the balance between ionization and attachment. This might happen when the ion kinetics are important, the attachment is partially or fully balanced by detachment, so the electron loss is reduced, yielding a higher effective ionization coefficient, and thus also a lower critical breakdown electric field, as is clear from Fig. 10(b).

As mentioned above, the traditional definition of the effective ionization coefficient in literature [25]-[33] only considers the electron kinetics, i.e. the balance between the reduced ionization coefficient (α) and the reduced attachment coefficient (η), as presented in Fig. 8. However, in our current study, we take into account both the electron and ions kinetics, by calculating the effective ionization coefficient with formula (10), and this leads to clear differences in the effective ionization rate coefficient and thus in the critical reduced breakdown electric field, as illustrated in Fig.10 (cf. curve 3 vs. curves 1 and 2). This shows that the commonly accepted effective ionization coefficients in literature can be underestimated, and hence the critical reduced breakdown electric field strength can be overestimated, when the ion kinetics are important.

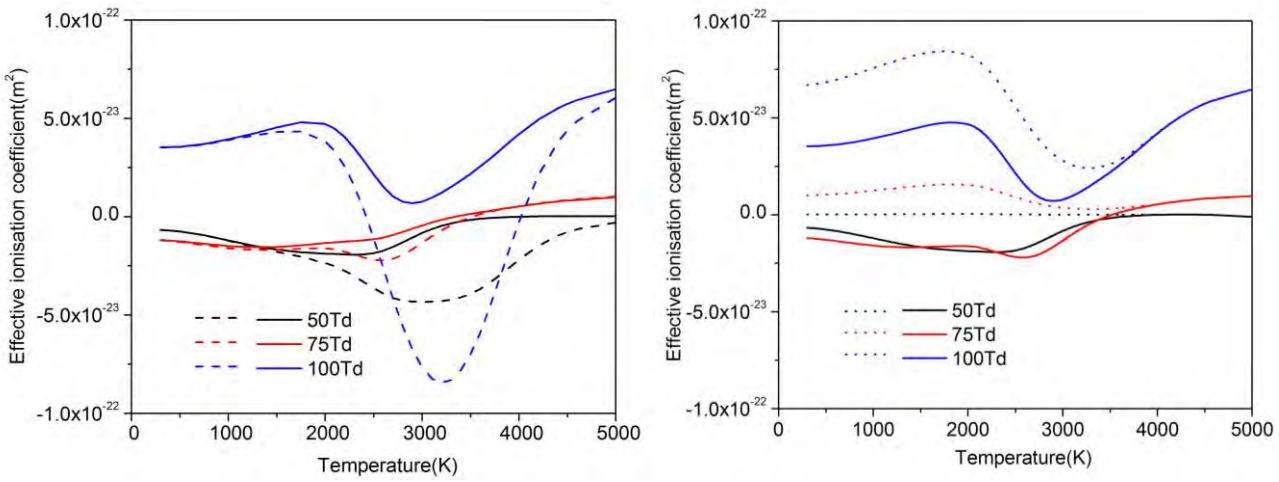

Fig.11 Effective reduced ionization coefficient (α_{eff}/N) of CO_2 (and its mixture of dissociation products),

as a function of gas temperature, at reduced electric field strengths of 50 Td, 75 Td and 100 Td and atmospheric pressure, with equilibrium ion composition (a) and overpopulated ion composition (b), including the vibrational kinetics with the Fridman approximation. Solid line: defined according to equation (10); dashed line: defined by ((α-η)/N), dotted line: defined considering the balance between ionization and recombination.

Fig. 11 presents the effective reduced ionization coefficients as a function of gas temperature, at reduced electric field strengths of 50 Td, 75 Td and 100 Td, and atmospheric pressure, both with an equilibrium ion composition (a) and an overpopulated ion composition (b). A comparison is made between the values calculated with the formula (10), thus accounting for all electron and ion kinetics, and the values obtained from the balance between ionization and attachment, as well as the balance between ionization and recombination.

As is indicated in Fig. 11(a), at 50Td and 75Td, and below around 1500 K, the ion kinetics (i.e., electron detachment in this case) has a negligible influence on the effective reduced ionization coefficient of CO_2, because the CO_2 dissociation is quite weak, so the main reactant for electron detachment (i.e., CO) has a too low density, and thus, the detachment rate is much smaller than the attachment rate, and the effective reduced ionization coefficient is simply determined by the balance between ionization and attachment, explaining why the solid and dashed curves coincide up to 1500 K in Fig. 11(a). Above 1500 K, the CO concentration reaches a level where the electron detachment of O^- upon collision with CO can effectively compete with CO_3^- cluster formation, and this process gradually reduces the importance of electron attachment as electron loss mechanism, thus affecting the effective ionization coefficient. Consequently, a deviation in the effective reduced ionization coefficients, calculated with and without ion kinetics, becomes apparent above 1500K (see Fig. 11(a)). At 100 Td, there is a very large deviation of the effective reduced ionization coefficient with and without accounting for the ion kinetics in the temperature range from 2000 K to 4000 K where the concentration of molecular oxygen reaches a relatively high value (see Fig.1). Without accounting for the ion kinetics, the effective reduced ionization coefficient is largely negative due to the very high dissociative electron attachment rate of molecular oxygen (mainly attributed to the vibrationally exited states). If the ion kinetics is taken into account, the electron loss due to electron attachment is greatly reduced by electron detachment, resulting in a positive value of the effective reduced ionization coefficient.

Fig. 11(b) shows that below 3500 K there is quite some deviation between the effective reduced ionization coefficients calculated when fully accounting for the ion kinetics (solid lines) and the effective ionization coefficients calculated from the balance between ionization and recombination (dotted lines), indicating that electron-ion recombination is not the dominant loss process, at temperatures below 3500 K. However, above this temperature, the dominant electron loss mechanism changes from electron attachment to electron-ion recombination, as soon as a balance between the electron attachment and detachment rate is reached. This means that the net contribution of electron loss by electron attachment is greatly reduced by the

electron detachment process, and electron-ion recombination is more important as electron loss mechanism. This explain why the curves of the effective ionization coefficients by considering the balance between ionization and recombination coincide with the curves obtained from the full definition of the effective reduced ionization coefficient, calculated with formula (10) for temperatures above 3500 K; see Fig. 11(b).

In summary, we can conclude that at reduced electric fields in the order of 50-100 Td, and temperatures below 1500 K, the ion kinetics seems negligible, and the effective ionization coefficient is simply determined by the balance between ionization and attachment. At higher temperatures, the ion kinetics cannot be neglected, and electron detachment reduces the role of electron attachment as electron loss process, so that electron-ion recombination starts playing a role. Upon increasing temperature, electron-ion recombination becomes gradually more important than electron attachment as electron loss process, and above 3500 K, it is the dominant electron loss mechanism, and thus the effective ionization coefficient can simply be determined by the balance between ionization and electron-ion recombination.

The critical reduced breakdown electric field strengths can be deduced from the electric field where the effective ionization coefficient reaches zero in Figs 9 and 10. Fig. 9 (a) shows that at 2500 K, this critical reduced breakdown electric field is about 96 Td, while at 4500K, the value is equal to 56 Td, 46 Td and 50 Td, respectively, in case of neglecting the vibrational and electronically excited levels of all species, and when including the vibrational levels with either the ground state approximation or the Fridman approximation (see Fig. 9(b)). For comparison, the reduced electric field at which the curves of the reduced ionization coefficients cross the curves of the reduced attachment coefficients in Fig. 8, corresponds to the critical value considering only the electrons kinetics. This yields a value of 103.5 Td at 2500 K (see Fig. 8(a)) and of 79 Td at 4500 K (see Fig. 8(b)). The difference between both definitions again shows that the ion kinetics play a significant role in determining the critical reduced breakdown electric field strength.

5.3 Critical Breakdown Electric Field Strength

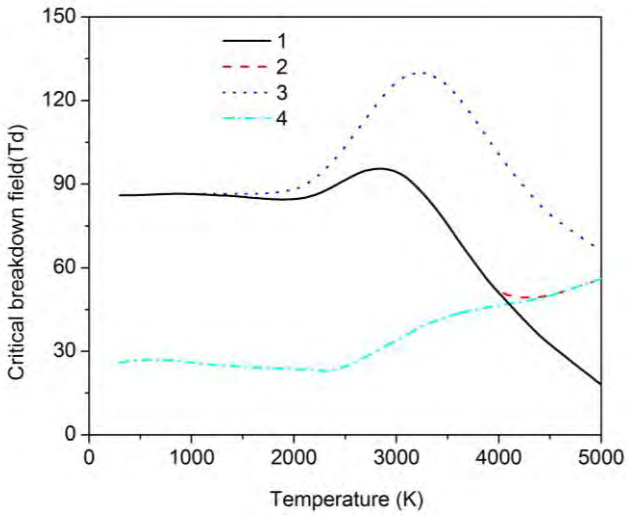

Fig.12 Calculated values of the critical reduced breakdown electric field in CO_2 (and its mixture of dissociation products) at atmospheric pressure, including the vibrational kinetics with the Fridman approximation. (1) Considering the full ion kinetics using the equilibrium ion composition; (2) Considering the full ion kinetics using an overpopulated ion composition; (3) Considering only the balance between electron impact ionization and attachment; (4) Considering the balance between ionization and electron-ion recombination.

Fig. 12 illustrates the calculated values of the critical reduced breakdown electric field strength (E_{cr}/N) in CO_2 as a function of gas temperature at atmospheric pressure, including the vibrational kinetics with the Fridman approximation. Below the temperature of 4000 K, there is no difference between the equilibrium and overpopulated ion composition (lines 1 and 2) but above 4000 K, the equilibrium ion composition yields a significant drop in the critical reduced breakdown electric field upon increasing temperature (see line 1), while the overpopulated ion composition leads to a slight increase in the values of the critical reduced breakdown electric field (line 2). Indeed, the overpopulated ion composition results in electron loss by electron-ion recombination, thus reducing the net electron production, resulting in a higher critical reduced breakdown electric field, while the equilibrium ion composition does not give rise to electron loss by electron-ion recombination (see formula 11), so the net electron production (by ionization) is much higher, resulting in a much lower critical reduced breakdown electric field.

It is also clear that the gas composition can greatly influence the critical breakdown electric field strength. At room temperature up to 1500 K, our model, including the vibrational and ion kinetics, predicts that E_{cr}/N = 86 Td (see line 2). At higher temperatures, the dissociation of CO_2 starts to occur, and the collision between CO and O^- ions, leading to electron detachment, starts to become more important than the CO_3^- cluster formation from O^- ions, thus, the production rate of electrons increases and this causes a slight drop in the critical breakdown electric field strength when considering both the electron and ion kinetics. In the temperature range between 2200 K and 2800 K, we notice a slight increase in the reduced critical breakdown electric field strength due to the formation of the dissociation product O_2, which has a higher attachment cross section, thus increasing the electron loss, and this gives rise to a slightly higher critical reduced breakdown electric field strength of 96 Td. In the temperature range from 2800 K to 4000 K, the value of E_{cr}/N dramatically decreases upon increasing gas temperature, mainly caused by the dissociation of CO_2 into CO and O_2 and further into O atoms. Especially above 3500 K, CO and O become dominant (see Fig. 1), and the value of E_{cr}/N becomes quite small. This can be explained because CO and O both have negligible or limited electron attachment cross sections. Thus, the loss of electrons by attachment is much lower than the electron production by ionization, yielding a lower critical reduced breakdown electric field. Moreover, above around 4000K, electron attachment is effectively balanced by electron detachment upon collision between O^- ions and CO, and thus the O^- ions generated by electron impact attachment are immediately converted back into electrons. Electron-ion recombination will then be the dominant electron loss mechanism.

Fig. 12 also shows the calculated critical reduced breakdown electric field strength without considering the ion kinetics, but simply obtained by the balance between ionization and attachment (line 3) and by the balance between ionization and electron-ion recombination (line 4). The classical definition of E_{cr}/N using a balance of electron impact ionization and attachment, which is most often used in literature [25]-[33], can predict the critical reduced electric field strength very well in the low temperature range below 1500K, but above this temperature, this classical definition predicts significantly higher values than the ones calculated with the full ion kinetics. Likewise, the balance between ionization and electron-ion recombination largely underestimates the critical reduced breakdown electric field up to a temperature of 4000K, simply because electron-ion recombination is negligible up to this temperature. However, at higher temperatures, it becomes the dominant electron loss mechanism, and thus, it yields a good agreement with the critical reduced breakdown electric field calculated by the full ion kinetics.

By comparing our predicted values with literature data, it is clear that the calculated reduced breakdown electric field at room temperature (86 Td) shows very good agreement with measurements (around 85 Td) [82]. Additionally, our calculations indicate that a higher temperature leads to a reduction of the reduced breakdown electric field in CO_2. This is also reported in literature based on experimental measurements. In [83] a voltage was applied to CO_2 gas at high temperature through a set of two rod electrodes made of stainless steel with a diameter of 1mm at atmospheric pressure. At 4000 K, a breakdown voltage of 55 V was measured and this corresponds to a reduced breakdown electric field of around 32 Td, which is a great drop compared to the value at room temperature. In their work, the gas temperature is determined by the energy conservation equation assuming the thermally equilibrium condition. Our calculated breakdown electric field (49 Td) considering the full ion kinetics using the equilibrium ion composition, i.e. under a similar condition (black solid line) matches reasonably with the experimental value under similar conditions. Therefore, we will use this case as a reference (black solid line in Fig. 13 and 14) to indicate the influence of the excited states (Fig.13) and different pressures (Fig.14) on the calculated reduced breakdown electric field.

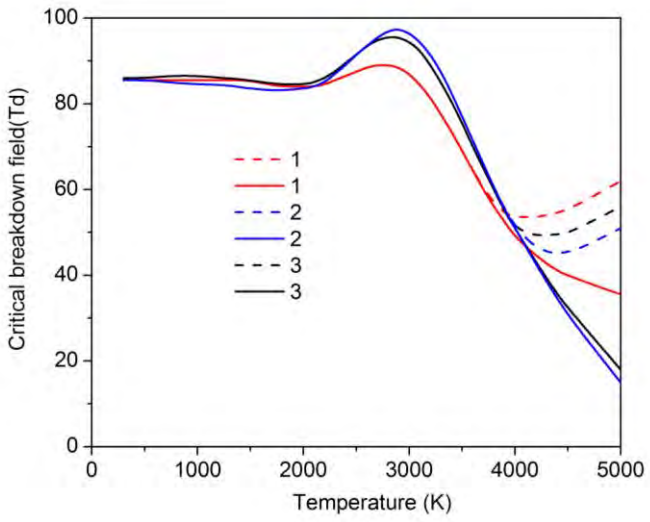

Fig. 13 Calculated values of the critical reduced breakdown electric field strength of CO_2 (and its mixture of dissociation products) at atmospheric pressure. Solid lines: using an overpopulated ion composition; dashed lines: using the equilibrium ion composition. (1) Neglecting the role of vibrational and electronically excited species; (2) Vibrational kinetics with ground state approximation; (3) Vibrational kinetics with Fridman approximation.

To investigate the effect of the excited species on the critical breakdown electric field, we plot in Fig.13 the values of the critical reduced breakdown electric field as a function of gas temperature, with and without considering the vibrational and electronically excited species. We also compare the ground state approximation and Fridman approximation when including the vibrational kinetics. The ion kinetics are accounted for, but a comparison is also made between assuming the equilibrium ion composition and a (two times) overpopulated ion composition.

It is clear that the vibrational and electronically excited species do not affect the critical breakdown electric field below about 2000 K due to their limited species concentrations compared with those of ground states. At around 3000K, when comparing the reference case (black solid line) with the case including only the ground states (red solid line), we can see that including the excited states yields a much higher critical breakdown electric field. This is mainly attributed to the contribution of vibrationally excited molecular oxygen, which results in a more pronounced increase in the dissociative electron attachment rate than in the ionization rate, due to the strong dependence of the dissociative attachment cross-sections on the vibrational quantum number [53]. Indeed, the vibrationally excited oxygen shows a rapid increase of the electron attachment cross section upon ring vibrational quantum number. Therefore, ignoring the role of the vibrationally excited states of molecular oxygen can bring an underestimation of the electrons loss rate by attachment. In contrast, the influence of vibrationally excited CO is minor due to the much smaller magnitude of their electron attachment cross section than those of O_2.

At higher temperature, including the excited states yields a somewhat lower critical breakdown electric field. The reason is that electron-ion recombination becomes the dominant electron loss mechanism, and its rate coefficient drops when including the excited states (mainly vibrational kinetics), while the ionization coefficient slightly rises, as illustrated in Fig. 8 above. This is both due to the broader EEDF, and thus somewhat higher electron energy, as a result of the superelastic collisions. Thus, including the vibrational kinetics yields a somewhat higher effective ionization coefficient, explaining the lower values of the critical breakdown electric field (as was also illustrated by the vertical dotted lines in Fig. 8 above). Moreover, the ground state approximation still yields somewhat lower values, because the ionization coefficient is somewhat higher and the recombination coefficient is somewhat lower (as explained in Fig. 8 above).

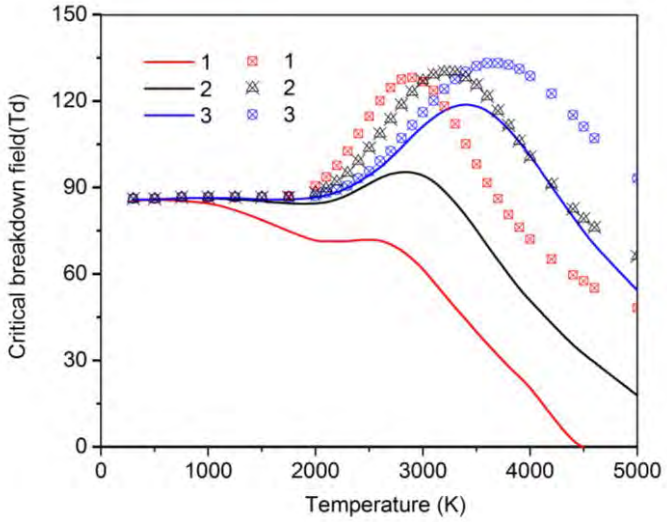

Fig.14 Calculated values of the critical reduced breakdown electric field strength of CO_2 (and its mixture of dissociation products) as a function of gas temperature and at different pressures, including the vibrational kinetics with the Fridman approximation, and based on the equilibrium ion composition. Solid lines: considering ion kinetics; symbols: considering only the electron kinetics, i.e., the balance between electron impact ionization and attachment. (1) 0.1 atm; (2) 1.0 atm; (3) 10 atm.

Finally, Fig. 14 shows the influence of different pressures on the critical reduced breakdown electric field as a function of temperature, considering the full ion kinetics as well as the simple balance between ionization and attachment. According to Le Chatelier's law, a higher pressure induces changes in the original state of equilibrium, so that dissociation is suppressed and shifted to a higher temperature (see Fig. 3 above). In the low temperature range (i.e., below 1000-2000 K), where dissociation does not occur, E_{cr}/N shows a rather weak dependence on the gas pressure, but above 2000 K, when comparing with the reference case at 1 atm (black solid line), a lower pressure of 0.1 atm (red solid line) leads to a faster drop in the Ecr/N upon increasing temperature, while at higher pressure of 10 atm (blue solid line) the values of Ecr/N stay longer constant or even rise upon higher temperature, as is obvious from Fig. 14. This rise in E_{cr}/N at higher pressure is due to the decreasing role of electron detachment upon higher pressure, resulting in a higher net electron loss due to electron attachment, and thus a higher critical reduced breakdown electric field. The subsequent drop in E_{cr}/N after the locally maximum value at 1 atm and 10 atm, which is already taking place at lower temperatures in case of the lower pressures, is due to the dissociation of CO_2 into CO and O_2, and subsequently into O atoms. Because electron attachment of CO and O is much more limited, this gives a higher net production of electrons, and thus a lower critical reduced breakdown electric field, as was also explained in Fig.12 above. The reason why this drop in E_{cr}/N occurs only at higher temperatures in case of the higher pressures is because dissociation, ionization and excitation are suppressed at higher pressure, so the dissociation products of CO_2 and the ions and excited species do not affect the effective ionization coefficient, until at a higher temperature.

The results obtained without considering the ions kinetics (see symbols in Fig. 14) lead to higher critical

reduced breakdown electric field strengths, simply because of the higher electron loss by electron attachment, as the latter is not compensated by electron detachment, and this higher electron loss yields a higher effective electron E_{cr}/N. More importantly, the deviation with the results obtained with full ion kinetics drops upon higher pressure, due to the decreasing role of electron detachment upon higher pressure. In general, we may conclude from Fig. 14 that increasing the gas pressure leads to a higher critical breakdown electric field at higher temperatures, and thus it can enhance the gas insulation performance of hot gases.

6. Conclusions

We calculated the effective ionization coefficients and critical reduced breakdown electric field strengths of CO_2 in the temperature range from 300 K to 5000 K, which occurs in many practical conditions, such as dielectric recovery during current interruption in a circuit breaker, as well as in a gliding arc. The equilibrium composition of a CO_2 mixture (i.e. CO_2 and its dissociation, ionization and excitation products) in this entire temperature range was calculated by means of Gibbs free energy minimization, considering the ground states as well as vibrationally and electronically excited states of the various molecules as independent species. The excited states are assumed to follow a Boltzmann distribution with a given excitation temperature. We applied a full set of cross sections, including the interaction between electrons and vibrationally and electronically excited states. The interactions between electrons and the dissociated (and excited) species of CO_2 in this wide temperature range are evaluated by the electron energy distribution function (EEDF) derived from the Boltzmann transport equation. We computed the effective ionization coefficient and the critical reduced breakdown electric field strength $(E/N)_{cr}$ of the hot gas mixture in this entire temperature range, based on the calculated composition, by balancing electron generation and loss processes. We investigated the effect of the excited states on the EEDF and on the effective ionization coefficient and the critical breakdown electric field, as well as the effect of the ion kinetics, including electron detachment from the negative ions initially created by electron attachment, cluster ion formation, charge transfer and electron-ion recombination.

Our results for the first time indicate that the ion kinetics play a significant role in determining the effective ionization coefficients and the critical reduced breakdown electric field strength of CO_2 at temperatures above 1500 K, as the values calculated in this way are clearly different from the results obtained based on the simple balance between electron impact ionization and attachment, which is mostly used in literature [25]-[33]. This result is important because it can significantly affect the discharge inception threshold and behavior near the critical reduced breakdown electric field strengths.

With increasing gas temperature, electron detachment upon collision of CO with O^- increases and this reduces the effective electron attachment rate. Thus, the major electron loss mechanism gradually shifts from electron attachment to electron-ion recombination. Therefore, the effective ionization coefficients, considering only the balance between electron attachment and ionization, will be underestimated, and consequently, the critical breakdown electric field strength will be overestimated, in the higher temperature range, where the dissociation of CO_2 occurs (i.e. above 1500K). Above 4000 K, electron-ion recombination becomes the

dominant electron loss mechanism, and thus plays an important role in the determination of the effective ionization coefficient and hence the critical breakdown electric field, when the ions is overpopulated, which is often the case in non-equilibrium plasma.

An increasing pressure can suppress the dissociation of CO_2, and this reduces the deviation of the calculated critical reduced breakdown electric field strength with and without ions kinetics. Moreover, a higher pressure yields a higher critical breakdown electric field, and can thus enhance the gas insulation performance of hot gases, which may be important for practical applications.

Furthermore, besides the effect of the ion kinetics, our work for the first time investigates the influence of excited states on the effective ionization coefficient and on the critical reduced breakdown electric field strength, in this high temperature range where the dissociation of CO_2 takes place. It is found that the rapid increase of the dissociative electron attachment cross-section of molecular oxygen upon rising vibrational quantum number causes a larger electron loss rate and thus enhances the critical reduced breakdown electric field strength in the temperature range where the concentration of molecular oxygen is relatively high. Our results also show that the excited species, lead to a greater population of high-energy electrons due to superelastic collisions, and this can enhance the effective ionization coefficient and thus reduce the critical breakdown electric field strength at high temperature (i.e., above ca. 4000K) where electron-ion recombination is the dominant electron loss mechanism.

The results obtained in this work, which shows reasonable agreement with literature experimental results, are important for the evaluation of the dielectric strength of CO_2 in a highly reactive environment at elevated temperature, for example, for the assessment of the post-arc dielectric recovery ability in the circuit breaker, as well as for studying the restrike and back-breakdown phenomena in a gliding arc.

Acknowledgements

This research was supported by the European Marie Skłodowska-Curie Individual Fellowship "GlidArc" within Horizon2020 and the FWO project (grant G.0383.16N). The computational work was carried out using the Turing HPC infrastructure at the CalcUA core facility of the Universiteit Antwerpen (UA), a division of the Flemish Supercomputer Center VSC, funded by the Hercules Foundation, the Flemish Government (department EWI) and the UA.

Reference

[1] W Z Wang, J D Yan, M Z Rong, A B Murphy, J W Spencer 2013 Theoretical investigation of the decay of an SF_6 gas-blast arc using a two-temperature hydrodynamic model *J. Phys. D: Appl. Phys* **46** 065203.

[2] L Rothhardt, J Mastovsky, G Jahn and J Blaha 1981 Breakdown experiments in air and nitrogen above 1500K *J. Phys. D: Appl. Phys*. **14** 715–21.

[3] M Seeger, G Naidis, A Steffens, H Nordborg and M Claessens 2005 Investigation of the dielectric recovery in synthetic air in a high voltage circuit breaker *J. Phys. D: Appl. Phys.* **38** 1795.

[4] A Indarto et al 2007 Gliding arc plasma processing of CO_2 conversion *J. Hazard. Mater.* **146** 309.

[5] Nunnally T, Gutsol K, Rabinovich A, Fridman A, Gutsol A and Kemoun A 2011 Dissociation of CO_2 in a low current gliding arc plasmatron *J. Phys. D: Appl. Phys.* **44** 274009.

[6] Thomas W R L 1969 The determination of the total excitation cross section in neon by comparison of theoretical and experimental values of Townsend's primary ionization coefficient *J. Phys. B: At. Mol. Opt. Phys.* **2** 551–61

[7] Tagashira H, Sakai Y and Sakamoto S 1977 The development of electron avalanches in argon at high E/N values: II. Boltzmann equation analysis *J. Phys. D: Appl. Phys.* **10** 1051–63.

[8] Taniguchi T, Tagashira H and Sakai Y 1978 Boltzmann equation analysis of the electron swarm development in nitrogen *J. Phys. D: Appl. Phys.* **11** 1757–68

[9] Kline L E, Davies D K, Chen C L and Chantry P J 1979 Dielectric properties for SF_6 and SF_6 mixtures predicted from basic data *J. Appl. Phys.* **50** 6789–96.

[10] Itoh H, Shimozuma M and Tagashira H 1980 Boltzmann equation analysis of the electron swarm development in SF_6 and nitrogen mixtures *J. Phys. D: Appl. Phys.* **13** 1201–9.

[11] Phelps A V and Van Brunt R J 1988 Electron-transport, ionization, attachment, and dissociation coefficients in SF_6 and its mixtures *J. Appl. Phys.* **64** 4269–77.

[12] Christophorou L G, Mathis R A, Hunter S R and Carter J G 1988 Effect of temperature on the uniform field breakdown strength of electronegative gases *J. Appl. Phys.* **63** 52–9.

[13] Christophorou L G and Van Brunt R J 1995 SF_6/N_2 mixtures: basic and HV insulation properties *IEEE Trans. DEI* **1** 952.

[14] Bordage M C, Segur P, Christophorou L G and Olthoff J K 1999 Boltzmann analysis of electron swarm parameters in CF_4 using independently assessed electron-collision cross sections *J. Appl. Phys.* **86** 3558–66.

[15] Kurihara M, Petrovic Z L and Makabe T 2000 Transport coefficients and scattering cross-sections for plasma modelling in CF_4–Ar mixtures: a swarm analysis *J. Phys. D: Appl. Phys.* **33** 2146–53.

[16] J de Urquijo, E Basurto and J L Hernández-Á vila 2003 Measurement of electron drift, diffusion, and effective ionization coefficients in the SF_6–CHF_3 and SF_6–CF_4 gas mixtures *J. Phys. D: Appl. Phys.* **36** 3132-7.

[17] Liu X L and Xiao D M 2007 Monte Carlo Simulation of Electron Swarm Parameters in the SF_6/CF_4 Gas Mixtures *Japanese Journal of Applied Physics* **46** 1663–7.

[18] Eliasson B and Schade E 1977 Electrical breakdown of SF_6 at high temperatures (<2300 K) *Proc. 13th Int. Conf. Phenomena in Ionized Gases (Berlin)* pp. 409–10.

[19] Schade E 1985 Recovery of switching arcs *Proc. 17th Int. Conf. Phenomena in Ionized Gases (Budapest)* pp. 277–97.

[20] Rothhardt L, Mastovsky J and Blaha J 1981 Dielectric strength of SF_6 at elevated temperatures *J. Phys. D: Appl. Phys.* **14 L** 215–6

[21] Rothhardt L, Mastovsky J and Blaha J 1985 Breakdown experiments in diluted SF_6 at elevated temperatures *J. Phys. D: Appl. Phys.* **18** L155–7

[22] Rothhardt L, Mastovsky J, Jahn G and Blaha J 1981 Breakdown experiments in air and nitrogen above 1500K *J. Phys. D: Appl. Phys.* **14** 715–21

[23] Uchii T, Iwata K, Kawano H, Nakamoto T, and Suzuki K 2001 Behaviour in Inhomogeneous High-temperature SF_6 Gas in a Gas Circuit Breaker *IEEE Power-Eng. Society Winter Meeting Conference Proc.* Vol. 1, pp. 289-94.

[24] Yan J D, Fang M T C and Liu Q S 1997 Dielectric breakdown of a residual SF_6 plasma at 3000K under diatomic equilibrium *IEEE T DIELECT EL IN* **4** 114–9

[25] Cliteur G J, Hayashi Y, Haginomori E and Suzuki K 1998 Calculation of the uniform breakdown field strength of SF_6 gas *IEEE T DIELECT EL IN* **5** 843–9.

[26] Yousfi M, Robin-Jouan Ph, Kanzari Z 2004 Breakdown Electric Field Calculations of Hot SF_6 for High Voltage Circuit Breaker Applications *IEEE T DIELECT EL IN* **12** 1192-200.

[27] Robin-Jouan Ph, Yousfi M 2007 New Breakdown Electric Field Calculation for SF_6 High Voltage Circuit Breaker Applications *Plasma Sci. Technol.* **9** 690-4

[28] Tanaka Y 2004 Prediction of dielectric properties of N_2/O_2 mixtures in the temperature range of 300–3500K *J. Phys. D: Appl. Phys.* **37** 851–9.

[29] Tanaka Y 2005 Influence of copper vapor contamination on dielectric properties of hot air at 300-3500 K in atmospheric pressure *IEEE T DIELECT EL IN* **12** 504-12.

[30] Zhao H, Li X W, Jia S L, Murphy A B 2013 Dielectric breakdown properties of SF_6–N_2 mixtures at 0.01–1.6 MPa and 300–3000 K *J. Appl. Phys.* **113** 143301.

[31] Wang W Z, Murphy A B, Rong M Z et al. 2013 Investigation on critical breakdown electric field of hot sulfur hexafluoride/carbon tetrafluoride mixtures for high voltage circuit breaker applications *J. Appl. Phys.* **114** 103301.

[32] Zhong L L, Yang A J, Wang X H et al. 2014 Dielectric breakdown properties of hot SF_6-CO_2 mixtures at temperatures of 300–3500 K and pressures of 0.01–1.0 MPa *Phys. Plasmas* **21** 053506.

[33] Sun H, Rong M Z, Wu Y et al. 2015 Investigation on critical breakdown electric field of hot carbon dioxide for gas circuit breaker applications *J. Phys. D: Appl. Phys.* **48** 055201.

[34] Colonna G, Capitelli M, Gorse C , Paniccia F, Eletskij AV and Smirnov B M 1992 Breakdown Conditions and Thermal Instability in Air *Nuovo Cimento D* **14** 585-593.

[35] Pietanza L D, Colonna G, D'Ammando G, Laricchiuta A, and Capitelli M. 2016 Electron energy distribution functions and fractional power transfer in “cold” and excited CO_2 discharge and post discharge conditions *Phys. Plasmas* **23** 013515.

[36] Pietanza L D, Colonna G, D'Ammando G, Laricchiuta A, and Capitelli M 2016 Non equilibrium vibrational assisted dissociation and ionization mechanisms in cold CO_2 plasmas *Chemical Physics* **468** 1

[37] Suzuki I 1968 General anharmonic force constants of carbon dioxide *J. Mol. Spectrosc.* **25** 479-500.

[38] Murphy A B 2001 Thermal plasmas in gas mixtures *J. Phys. D: Appl. Phys.* **34** 151-73.

[39] Wang W Z, Rong M Z, Wu Y and Yan J D 2014 Fundamental properties of high-temperature SF_6 mixed with CO_2 as a replacement for SF_6 in high-voltage circuit breakers *J. Phys. D: Appl. Phys*. **47** 255201.

[40] Colonna G, Capitelli M, De Benedictis S, Gorse C and Paniccia F 1991 Electron energy distribution functions in CO_2 laser mixture: the effects of second kind collisions from metastable electronic states *Contrib. Plasma Phys.* **31** 575–579.

[41] Capitelli M, Colonna G, Hassouni K, Gicquel A 1994 Electron energy distribution functions in non-equilibrium H_2 discharges. The role of superelastic collisions from electronically excited states *Phys. Chem. Lett.* **228** 687-694.

[42] Lowke J J, Phelps A V and Irwin B W 1973 Predicted electron transport coefficients and operating characteristics of CO_2–N_2–He laser mixtures *J. Appl. Phys.* **44** 4664.

[43] Phelps database, www.lxcat.net, retrieved on January 17, 2016. Lawton S A and Phelps AV 1978 Excitation of the b 1Σ+ g state of O_2 by low energy electrons *J. Chem. Phys.* **69** 1055.

[44] Phelps database, www.lxcat.net, retrieved on January 17, 2016. Hake R D and Phelps A V Momentum-transfer and inelastic-collision cross sections for electrons in O_2, CO, and CO_2 1967 *Phys. Rev.* **158** 70-8

[45] Itikawa database, www.lxcat.net, retrieved on January 17, 2016. Itikawa Y 2002 Cross Sections for Electron Collisions With Carbon Dioxide *J. Phys. Chem. Ref. Data* **31** 749.

[46] Pietanza LD, Colonna G, Laporta V, Celiberto R, D'Ammando G, Laricchiuta A, Capitelli M 2016 Influence of electron molecule resonant vibrational collisions over the symmetric mode and direct excitation-dissociation cross sections of CO_2 on the electron energy distribution function and dissociation mechanisms in cold pure CO_2 plasmas *J Phys Chem A*. **120** 2614-2628.

[47] Cosby P C, Helm H 1993 Dissociation rates of diatomic molecules *Report AD-A266* **464** WL-TR-93-2004.

[48] Land J E 1978 Electron scattering cross sections for momentum transfer and inelastic excitation in carbon monoxide *J. Appl. Phys.* **49** 5716

[49] Laporta V, Tennyson J and Celiberto R 2016 Carbon monoxide dissociative attachment and resonant dissociation by electron-impact *Plasma Sources Sci. Technol*. **25** 01LT04.

[50] Janev R K and Reiter D 2003 Collision process of hydrocarbon species in hydrogen plasmas. Part 1. The methane family *ChemInform* **34** (doi:10.1002/chin.200325274).

[51] Janev R, Wang J, Murakami I and Kato T 2001 NIFS-DATA vol 68.

[52] Kosarim A V, Smirnov B M, Capitelli M, Laricchiuta A, PanicciaElectron F 2006 impact ionization cross sections of vibrationally and electronically excited oxygen molecules *Chem. Phys. Lett.* **422** 513–517.

[53] Laporta V, Celiberto R,and Tennyson J 2015 Dissociative electron attachment and electron-impact resonant dissociation of vibrationally excited O_2 molecules *Phys. Rev. A* **91** 012701.

[54] Liu C, Eliasson B, Xue B, Li Y and Wang Y 2001 Zeolite-Enhanced Plasma Methane Conversion Directly to Higher Hydrocarbons Using Dielectric-Barrier Discharges *React. Kinet. Catal. Lett.* **74** 71.

[55] Eliasson B and Kogelschatz U 1986 Basic data for modelling of electrical discharges in gases: oxygen *Brown Boveri Research Report* KLR 86-11C.

[56] Matejcik S, Kiendler A, Cicman P, Skalny J, Stampfli P, Illenberger E, Chu Y, Stamatovic A and M¨ark T D 1997 Electron attachment to molecules and clusters of atmospheric relevance: oxygen and ozone *Plasma Sources Sci. Technol.* **6** 140.

[57] Morgan database, www.lxcat.net, retrieved on April 7, 2016.

[58] Eliasson B, Hirth M, and Kogelschatz U 1987 Ozone Synthesis from Oxygen in Dielectric Barrier Discharges *J. Phys. D: Appl. Phys.* **20** 1421-1437.

[59] O' Malley T F 1967 Calculation of Dissociative Attachment in Hot O_2 *Phys. Rev.* **155** 59-63.

[60] Database of the European Union phys4entry project 2012–2015 http://users.ba.cnr.it/imip/cscpal38/phys4entry/database.html

[61] Ionin A A, Kochetov I V, Napartovich A P and Yuryshev N N 2007 Physics and engineering of singlet delta oxygen production in low-temperature plasma *J. Phys. D: Appl. Phys.* **40** R25-R61.

[62] Pandya S H and Joshipura K N 2014 Ionization of metastable nitrogen and oxygen atoms by electron impact: Relevance to auroral emissions *J. Geophys. Res. Space Physics* **119** 2263–2268.

[63] Jelenaka A, Jovanović J V et al, 1995 The influence of excited states on the kinetics of excitation and dissociation in gas mixtures containing methane *Diamond and Related Materials* **4** 1103–12

[64] Fridman A 2008 Plasma Chemistry (Cambridge: Cambridge University Press).

[65] Celiberto R, Capitelli M, and Janev R K 1996 Scaling of electron-impact electronic excitation cross sections of vibrationally excited diatomic molecules *Chemical Physics Letters* **256** 575-580.

[66] William L Nighan and Wiegand W J 1974 Influence of negative-ion processes on steady-state properties and striations in molecular gas discharges *Physical Review A* **10** 922.

[67] Verhaart H F A and van der Laan P C T 1984 The influence of water vapour on avalanches in air *J. Appl. Phys.* 55 3286.

[68] Pancheshnyi S 2013 Effective ionization rate in nitrogen–oxygen mixtures *J. Phys. D: Appl. Phys.* **46** 155201.

[69] Hagelaar G J M and Pitchford L C 2005 Solving the Boltzmann equation to obtain electron transport coefficients and rate coefficients for fluid models *Plasma Sources Sci. Technol.* **14** 722–733

[70] Rockwood S D 1973 Elastic and Inelastic Cross Sections for Electron-Hg Scattering from Hg Transport Data *Phys. Rev. A* **40** 399.

[71] Hokazono H and Fujimoto H 1987 Theoretical analysis of the CO_2 molecule decomposition and contaminants yield in transversely excited atmospheric CO_2 laser discharge *J. Appl. Phys.* **62** 1585.

[72] Beuthe T G and Chang J S *1997 Chemical kinetic modelling of non-equilibrium Ar–CO_2 thermal plasmas Japan. J. Appl. Phys.* **36** 4997.

[73] Liu W and Victor G A 1994 Electron energy deposition in carbon monoxide gas *Astrophys. J.* **435** 909.

[74] Eliasson B, Hirth M and Kogelschatz U 1987 Ozone synthesis from oxygen in dielectric barrier discharges *J. Phys. D: Appl.Phys.* **20** 1421

[75] Capitelli M, Ferreira C M, Gordiets B F and Osipov A I 2000 *Plasma Kinetics in Atmospheric Gases*, Springer-Verlag, Berlin.

[76] Gudmundsson J T and Thorsteinsson E G 2007 Oxygen discharges diluted with argon: dissociation processes *Plasma Sources Sci. Technol.* **16** 399

[77] Cenian A, Chernukho A and Borodin V 1995 Modeling of Plasma-Chemical Reactions in Gas Mixture of CO_2 Lasers I. Gas Decomposition in Pure CO_2 Glow Discharge *Contrib. Plasma Phys.* **35** 273

[78] Ionin A A, Kochetov I V, Napartovich A P and Yuryshev N N 2007 Physics and engineering of singlet delta oxygen production in low-temperature plasma *J. Phys. D: Appl. Phys.* **40** R25.

[79] Wang W Z, Rong M Z, Wu Y, Spencer J W, Yan J D and Mei D H 2012 Thermodynamic and transport properties of two-temperature SF_6 plasmas *Phys. Plasmas* **19** 083506.

[80] Wang W Z, Rong M Z, Yan J D, Murphy A B, and Spencer J W 2011 Thermophysical properties of nitrogen plasmas under thermal equilibrium and non-equilibrium conditions *Phys. Plasmas* **18** 113502.

[81] Gleizes A, Mbolidi F and Habibt A A M 1993 Kinetic model of a decaying SF_6 plasma over the temperature range 12000 K to 3000 K *Plasma Sources Sci. Technoi.* **2** 173-179.

[82] Davies D K 1978 Ionization and attachment coefficients in CO_2: N_2: He and pure CO_2 *J. Appl. Phys.* **49** 127-131.

[83] Matsumura T, Yokomizu Y, Almiron P C and Shibuya M 2005 Breakdown Voltage of CO_2 at Temperatures around 4000K and in Range from 300 to 700K *IEEJ Transactions on Power and Energy* **125** 1063-1069.

Appendix 1

Table 3: Electron impact reactions described by collision cross sections, as well as the references where these cross sections were adopted from.

Process	Reaction	Ref.	Note
Elastic collision	$e^- + CO_2 \rightarrow e^- + CO_2$	[42]	a
Ionization	$e^- + CO_2 \rightarrow e^- + e^- + CO_2^+$	[42]	a
Dissociative ionization	$e^- + CO_2 \rightarrow e^- + e^- + CO^+ + O$	[45]	b
Dissociative ionization	$e^- + CO_2 \rightarrow e^- + e^- + C^+ + O_2$	[45]	b
Dissociative ionization	$e^- + CO_2 \rightarrow e^- + e^- + O^+ + C+O$	[45]	b
Dissociative attachment	$e^- + CO_2 \rightarrow e^- + O^- + CO$	[42]	b
Dissociation	$e^- + CO_2 \rightarrow e^- + CO+O$	[42]	b, c
Electronic excitation	$e^- + CO_2 \rightarrow e^- + CO_2el$	[42]	a
Vibrational excitation	$e^- + CO_2 \rightarrow e^- + CO_2v_i$ (i=1-8)	[42]	d
Elastic collision	$e^- + CO \rightarrow e^- + CO$	[48]	a
Ionization	$e^- + CO \rightarrow e^- + e^- + CO^+$	[48]	a
Dissociative ionization	$e^- + CO \rightarrow e^- + e^- + C^+ + O$	[48]	b
Dissociative ionization	$e^- + CO \rightarrow e^- + e^- + O^+ + C$	[48]	b
Electronic excitation	$e^- + CO \rightarrow e^- + COei$ (i=1-5)	[48]	a
Vibrational excitation	$e^- + CO \rightarrow e^- + COv_i$ (i=1-10)	[48]	d
Dissociative attachment	$e^- + CO \rightarrow e^- + O^- + C$	[49]	e
Elastic collision	$e^- + C \rightarrow e^- + C$	[50]	a
Ionization	$e^- + C \rightarrow e^- + e^- + C^+$	[50]	f
Electronic excitation	$e^- + C \rightarrow e^- + C(1D)$	[50]	
Electronic excitation	$e^- + C \rightarrow e^- + C(1S)$	[50]	f
Elastic collision	$e^- + C_2 \rightarrow e^- + C_2$	[51]	
Dissociation	$e^- + C_2 \rightarrow e^- + C+C$	[51]	
Ionization	$e^- + C_2 \rightarrow e^- + e^- + C_2^+$	[51]	
Elastic collision	$e^- + O_2 \rightarrow e^- + O_2$	[43]	a
Dissociation	$e^- + O_2 \rightarrow e^- + O+O$	[43]	b
Ionization	$e^- + O_2 \rightarrow e^- + e^- + O_2^+$	[52]	a
Dissociative ionization	$e^- + O_2 \rightarrow e^- + e^- + O + O^+$	[43]	b
Dissociative attachment	$e^- + O_2 \rightarrow O + O^-$	[53]	e
Attachment	$e^- + O_2 + M \rightarrow M + O_2^-$	[43]	a
Vibrational excitation	$e^- + O_2 \rightarrow e^- + O_2v_i$ (i=1-4)	[43]	d
Electronic excitation	$e^- + O_2 \rightarrow e^- + O_2ei$ (i=1-5)	[43]	a
Elastic collision	$e^- + O_3 \rightarrow e^- + O_3$	[54]	

Dissociation	$e^- + O_3 \rightarrow e^- + O_2 + O$	[55]	
Dissociative ionization	$e^- + O_3 \rightarrow e^- + e^- + O_2^+ + O$	[55]	
Dissociative ionization	$e^- + O_3 \rightarrow e^- + O^- + O^+ + O$	[55]	
Dissociative attachment	$e^- + O_3 \rightarrow O^- + O_2$	[56]	
Dissociative attachment	$e^- + O_3 \rightarrow O_2^- + O$	[56]	
Elastic collision	$e^- + O \rightarrow e^- + O$	[57]	a
Ionization	$e^- + O \rightarrow e^- + e^- + O^+$	[57]	h
Electronic excitation	$e^- + O \rightarrow e^- + O(1D)$	[57]	
Electronic excitation	$e^- + O \rightarrow e^- + O(1S)$	[57]	f
Attachment	$e^- + O + M \rightarrow M + O^-$	[58]	i

(a) Same cross section used for reactions of CO_2vi, and analogously for COvi or O_2vi

(b) Cross section modified by lowering the energy threshold by the excited state energy for reactions of CO_2vi, and analogously for COvi and O_2vi.

(c) Dissociation through electron impact excitation with 7.0 eV threshold.

(d) Cross section scaled and shifted for reactions of vibrationally excited states using Fridman's approximation, see equation (4).

(e) Cross section for the dissociative attachment of COvi and O_2vi obtained from the literature calculation in [49] and [53] respectively.

(f) Cross section modified by lowering the energy threshold by the excited state energy for reactions of excited carbon atoms.

(g) Cross section for the ionization reactions of COvi obtained from the literature by ab-initio model [52].

(h) Cross section for the ionization of the excited oxygen atoms obtained from the literature calculation in [59].

(i) A constant rate coefficient 1.00×10^{-31} cm^6 s^{-1} is used.

Appendix 2

Table 4 Ion kinetics as well as their rate coefficients and the references where these data were adopted from. The rate coefficients are in cm^3 s^{-1} for the two-body reactions, and in cm^6 s^{-1} for the three-body reactions.

Reaction type	Rate coefficient	Ref.
Electron-ion recombination		
$e^- + CO_2^+ \rightarrow CO + O$	$2.15\times10^{-3} T_e^{-0.50} / T_g$	[71]
$e^- + CO_2^+ \rightarrow C + O_2$	$1.66\times10^{-5} T_e^{-0.40}$	[72]
$e^- + CO^+ \rightarrow C + O$	$6.33\times10^{-6} T_e^{-0.55}$	[73]
$e^- + O^+ + M \rightarrow O + M$ (M = any neutral species)	$6.0\times10^{-27}(300/T_e)^{1.5}$	[74]
$e^- + O^+ + e^- \rightarrow O + e^-$	$7.0\times10^{-20}(300/T_e)^{4.5}$	[75]
$e^- + O_2^+ + M \rightarrow O_2 + M$	1.00×10^{-26}	[74]

$e^- + O_2^+ \rightarrow O+O$	$6.46\times10^{-5} T_e^{-0.50} T_g^{-0.50}$	[75]
Electron detachment		
$O^- + A \rightarrow CO_2 + e^-$ (A = CO, COei, COvi)	5.5×10^{-10}	[71]
$O^- + A \rightarrow O_2 + e^-$ (A = O, O(1S), O(1D))	2.3×10^{-10}	[76]
$O^- + A \rightarrow O_3 + e^-$ (A = O_2, O_2vi)	1.0×10^{-12}	[77]
$O^- + O_3 \rightarrow O_2 + O_2 + e^-$	3.0×10^{-10}	[78]
$O^- + A \rightarrow O_3 + e^-$ (A = O_2ei)	3.0×10^{-10}	[75]
$O^- + M \rightarrow O + M + e^-$ (M = any neutral species)	4.0×10^{-12}	[77]
$O_2^- + A \rightarrow O_3 + e^-$ (A = O, O(1S), O(1D))	3.3×10^{-10}	[76]
$O_2^- + A \rightarrow A + O_2 + e^-$ (A = O_2, O_2ei, O_2vi)	2.18×10^{-18}	[74]
$O_2^- + O_2ei \rightarrow O_2 + O_2 + e^-$	2.0×10^{-10}	[75]
$O_2^- + M \rightarrow O_2 + M + e^-$ (M = any other neutral species)	$2.70\times10^{-10}(T_g/300)^{0.50}\exp(-5590/T_g)$	[71]
Ion conversion		
$O^- + A + M \rightarrow CO_3^- + M$ (A = CO_2, CO_2ei, CO_2vi) (M = any neutral species)	9.0×10^{-29}	[75]
$O^- + A + M \rightarrow O_3^- + M$ (A = O_2, O_2ei, O_2vi) (M = any neutral species)	$3.00\times10^{-28}(T_g/300)^{-1.0}$	[77]
$O_2^- + O \rightarrow O^- + O_2$	3.0×10^{-10}	[77]

T_e: electron temperature, T_g: gas temperature ;

ei and vi mean the electronically and vibrationally excited states.